N-VEGF, the forgotten isoform of VEGF-A, activate cellular stress survival circuits

Marina Katsman[1], Aviva Azriel[1], Guy Horev[2] and Ben-Zion Levi[1*]

[1]Faculty of Biotechnology and Food Engineering, Technion-Israel, Institute of Technology, Haifa, Israel.
[2]Bioinformatics Knowledge Unit, The Lorry I. Lokey Interdisciplinary Center for Life Sciences and Engineering, Technion-Israel, Institute of Technology, Haifa, Israel.

*Corresponding author, e-mail: blevi@technion.ac.il

Abstract

Vascular Endothelial Growth Factor A (VEGF-A) is a major angiogenesis stimulator in response to hypoxia. Its first exon possesses an elongated 5' Untranslated Region (5'UTR) and two Internal Ribosome Entry Sites (IRESs), enabling translation under hypoxia. It also encodes a 180 aa peptide that is in-frame with the coding region of VEGF-A. Upon hypoxia, Long VEGF-A (L-VEGF) is translated from this reading-frame concomitant with canonical VEGF-A isoforms. L-VEGF is proteolytically cleaved upstream to the VEGF-A translation initiation site to generate N-VEGF, which under hypoxia shuttles to cells nuclei. Here we show by RNA-seq that hypoxia-independent nuclear mobilization of N-VEGF into NIH3T3 cells nuclei induced key genes associated with angiogenesis, cellular maintenance, and survival. Conversely, CRISPR-Cas9 mediated deletion of N-VEGF resulted in cells sensitive to hypoxia. Our results highlight the role of N-VEGF, the non-canonical VEGF-A isoform, in perpetuating the initial steps of angiogenesis along with the potentiation of cell survival circuits.

Introduction

Angiogenesis is the process of new blood vessel formation from pre-existing vasculature. VEGF-A (or VEGF) is a member of a family of proteins including VEGF-B, VEGF-C, VEGF-D, and VEGF-E that have a central role in mediating angiogenesis in normal physiology as well as in pathological events such as cancer (for review see [1, 2]). While VEGF is encoded by a single copy gene, many isoforms were identified due to alternative splicing. The 26 N-terminus amino acids (aa) of VEGF isoforms act as a signal peptide that is cleaved upon secretion [3, 4]. Being a major angiogenic factor, VEGF is subjected to multilevel regulation to ensure proper expression during embryogenesis and adulthood. The short-lived VEGF mRNA has a conserved and very long 5'UTR, 1038bps in human and 1014bps in mice, that is induced and stabilized upon stress signals such as hypoxia [5]. As shown by us and others, the long 5'UTR contains two IRES elements, A and B [6, 7] (see illustration in Fig. 1A). The 198 bps IRES A, is located at the 3’ end of this UTR, close to the VEGF translation initiation start site [6]. IRES B is about 400 bps in length and is located at the 5’ end of this UTR close to the transcription start site [8]. These two regulatory elements ensure efficient translation under stress conditions such as hypoxia, where normal translation *via* ribosomal scanning mechanism is severely impaired [9]. In addition, this 5'UTR also harbors a highly conserved ORF, which overlaps with IRES A. As shown by us, and confirmed by others,

this ORF adds 180 aa to the VEGF coding sequence to generate a Long VEGF isoform (L-VEGF) that is expressed in VEGF producing cells as well as in various cancer cells [10-12]. This L-VEGF is initiated by a CUG codon that mediates translation initiation and is followed by additional three conserved CUGs. We have shown that under hypoxia, L-VEGF is produced and subsequently subjected to a proteolytic cleavage upstream to VEGF classical translation start site. Consequently, the cleaved product translocates to the nuclei of expressing cells and is therefore coined N-VEGF due to an intrinsic non-classical Nuclear Localization Signal (NLS) confined to its 50 aa N-terminus [13]. Under normal conditions, constitutive ectopic expression of N-VEGF results in cytoplasmic expression, whereas upon hypoxia, this ectopically expressed N-VEGF shuttles only to the nuclei. [13]. Furthermore, immunohistochemical staining of normal angiogenic tissue samples such as kidney and breast demonstrated sporadic staining of N-VEGF in nuclei of renal tubular epithelium and in nuclei of epithelium cells coating the mammary ducts. Nuclei of the corresponding tumors samples taken from cancer patients, renal cell carcinoma and breast cancer, exhibited strong immunostaining of N-VEGF in all cells. Accordingly, Immunohistochemical staining of these normal and cancer tissues with anti-VEGF antibodies demonstrated cytoplasmic or extra cellular staining in the same cell types, confirming the coexpression of N-VEGF and VEGF [13, 14]. The nuclear function of N-VEGF is not known and was implicated in the control of the expression of a specific VEGF-A isoform [14].

In this study we provide direct evidence demonstrating a novel pivotal role of N-VEGF in the induction of regulatory circuits that are critical for cell maintenance and survival during hypoxic stress. Nuclear mobilization of N-VEGF without hypoxia as well as CRISPR-Cas9 mediated genomic deletion of N-VEGF followed by RNA-seq data analyses, indicated that at least 155 genes are regulated directly or indirectly by N-VEGF. These results add a new layer to the role of the VEGF gene during normal and pathological angiogenesis.

Results

Hypoxia-independent mobilization of N-VEGF to cells' nuclei

It is well documented that following hypoxia, a notable change occur in the transcriptome signature of the stressed cells [15]. As discussed above, the nuclear function of N-VEGF is not known and we hypothesize that N-VEGF, in addition to VEGF, is also involved in this stress mediated transcriptome-profile change promoting cells adaptation to the harsh environment imposed by the stress stimulus. To study the possible contribution of N-VEGF to this transcriptome-profile change, we chose to mobilize N-VEGF to cells nuclei avoiding hypoxia, which leads to the induction of notable and parallel regulatory pathways [15, 16]. For that purpose, we fused N-VEGF at its N-terminus to the NLS of the Cas9 nuclease (NLS-N-VEGF). N-VEGF and NLS-N-VEGF were cloned under the inducible Tet-on promoter in a lentiviral vector [17]. Subsequently, NIH3T3 cells were transduced with these two lentiviral vectors and antibiotic resistant cells were further cultivated. For controlled expression, these two cell types, expressing N-VEGF or NLS-N-VEGF, were grown in the presence or absence of the Tet-on promoter inducer, doxycycline (dox). Twenty-four hours later, cells were lysed, and cytoplasmic and nuclear fractions were prepared. Western blot analyses were performed on these cell lysate samples using our polyclonal antibodies directed against N-VEGF (for details see Materials and methods). As seen in Fig. 1B, under normoxia, residual levels of N-VEGF and NLS-N-VEGF were detected only in cytoplasmic fractions from cells that were not exposed to dox. This low level is probably due to the documented leakiness of the Tet-on promoter. As expected, a significant increase in the expression level of N-VEGF and NLS-N-VEGF was obvious in the cytoplasmic fractions of all cells treated with dox (Fig. 1B, compare lanes 1 and 2 with lanes 3 and 4, respectively). Yet, nuclear localization was observed only in cells expressing NLS-N-VEGF treated with dox (Fig. 1B, upper panel, lane 8). Although, a strong induction of NLS-N-VEGF was observed in the cytoplasm (Fig. 1B lane 4,), about~25% of the NLS-N-VEGF protein was detected in the nuclei of cells (for relative expression data, see Fig. S1). This also explains why residual NLS-N-VEGF expression was not detected in the nuclear fraction (Fig. 1B lane 6). Taken together, only the Cas9-NLS promoted nuclear expression of NLS-N-VEGF under normoxia following dox induction. The fact that not all cytoplasmic NLS-N-VEGF shuttled to the nucleus following dox induction, may be attributed to the N-terminal fused Cas9-NLS, which did not promote effective nuclear translocation possibly due to the N-terminal conformation of the N-VEGF protein. C-terminal fusion of Cas9-NLS was not possible since N-VEGF is cleaved from L-VEGF and the exact cleavage point within N-VEGF C-terminal coding frame is not known [13]. Finally, Ponceau S membrane staining and Western blot analyses were performed to show

that similar amounts of proteins were loaded on the gels and that the cytoplasmic and nuclear soluble proteins fractions were not cross contaminated during the purification procedure (Fig. S2).

Additionally, the nuclear expression of NLS-N-VEGF is best demonstrated by immunofluorescence staining of these two transduced cell types. Cells were grown in the presence of dox and were either subjected or not subjected to hypoxia. Nuclear or cytoplasmic N-VEGF staining was detected using our polyclonal antibodies directed against N-VEGF (for details see Materials and methods). It is clear that cells expressing N-VEGF exhibit nuclear localization only following hypoxia as denoted by the yellow coloring of the nuclei (Fig. 1C, second row, merge column). On the other hand, nuclear yellow staining is obvious in cells expressing NLS-N-VEGF regardless of hypoxia (Fig. 1C, third and fourth rows, merge column).

In conclusion, Cas9-NLS is driving NLS-N-VEGF nuclear expression regardless of hypoxia. Consequently, the contribution of N-VEGF alone to cellular transcriptome change can be evaluated without employing the hypoxic stress.

Hypoxia-independent mobilization of NLS-N-VEGF

To study the effect of nuclear NLS-N-VEGF on cellular transcriptome profile, RNA was extracted from cells expressing either N-VEGF or NLS-N-VEGF prior or following exposure to dox and subjected to RNA-Seq. The data was compiled as described briefly under Materials and methods. To identify differentially expressed genes as a result of the shuttling of N-VEGF to the nuclei, gene expression of NIH3T3 cells expressing NLS-N-VEGF with dox treatment was compared to that of cells transfected with N-VEGF with and without dox treatment and to cells transfected with NLS-N-VEGF without dox treatment. The differentially expressed genes were further divided to up and down regulated groups (adjusted p-value<0.05) and each group was functionally annotated using Metascape [18]. The data analysis (see Materials and methods) highlighted 155 genes that exhibited significant differential expression. Among them, 123 were upregulated and 32 genes were downregulated as a result of the shuttling of N-VEGF to NIH3T3 cells nuclei (see genes list in Table S1). The annotated groups of the upregulated genes are shown in Fig. 2A and are clustered into three main categories. The first category, represent genes associated with pathways supporting angiogenesis, pointing to the ability of N-VEGF to induce angiogenic signals similar to VEGF, but without the stress inducers. As seen in Fig. 2A, purple bars, seven of the annotated groups are included in this category such as: vascular development, angiogenesis, signaling by VEGF, response to oxidative stress, cellular response to hypoxia and vasoconstriction. The second category is associated with cell response to stress by regulating apoptosis to

avoid cell death (Fig. 2A, brown bars). The three major annotated groups included in this category are negative regulation of apoptotic signaling, negative regulation of extrinsic apoptotic pathway, and apoptotic signaling pathway. The last and major category of annotated gene groups are associated with maintenance of cellular structure during the hypoxic stress (Fig. 2A, red bars). For example, focal adhesion, actin cytoskeleton organization, actin filament-based process, actin filament organization, positive regulation of cell adhesion and more. Taken together, nuclear mobilization of N-VEGF results in inducing regulatory pathways that on one hand are associated with angiogenesis and on the other hand are engaged with the cell's ability to elicit cellular rescue pathways following stress signaling such as hypoxia, even in the absence of hypoxia. The downregulated genes following the mobilization of NLS-N-VEGF to the nucleus are annotated to groups such as regulation of translation, cell development, response to oxidative stress, protein ubiquitination, metabolism of carbohydrate and post-transcriptional regulation of gene expression (Fig. 2B). This fits with the role of N-VEGF as inducer of cell's adaptive mechanism to hypoxic crisis.

To validate the RNA-seq results, real-time RT-qPCR analyses were performed on selected genes from each functional annotation group. For the sake of simplicity, the data is presented for NLS-N-VEGF expressing cells before and following treatments with dox or dox combined with hypoxia (Fig. 3 light blue, blue, and dark blue columns, respectively). It is compared to control NIH3T3 cells before and following hypoxia (light green and dark green columns, respectively). From the data shown in Fig. 3, it is clear that the RT-qPCR results are consistent with RNA-seq data. Moreover, it is important to note that the expression magnitude of these selected genes in untransfected NIH3T3 cells following hypoxia follows the same trend, upregulated or downregulated (Fig. 3, compare light green to dark green columns). However, the level of induced\repressed mRNA in NLS-N-VEGF cells following dox treatment and hypoxia is significantly higher\lower (Fig. 3, compare dark blue columns to other columns). This is probably due to the concurrent nuclear presence of both ectopic and intrinsic expression of N-VEGF.

Taken together, this data demonstrates that cells expressing N-VEGF independent of hypoxia are executing partial hypoxia like response manifested by limited gene induction profile similar to the profile in untransfected NIH3T3 cells subjected to hypoxia. This comparison between hypoxia independent genes induction in NLS-N-VEGF expressing cells and NIH3T3 cells following hypoxia was further expanded using RNA-seq analysis (detailed hereafter, Fig. 7).

Genomic deletion of N-VEGF using CRISPR-Cas9

To show the significance of N-VEGF for cell physiology before and following hypoxia, we took advantage of the CRISPR-Cas9 genome editing system to delete only the coding region of N-VEGF (178 aa in mice) without affecting the translation start site of the "classical" VEGF. The 5'UTR of VEGF harbors two IRESs, 5'IRES B and 3'IRES A (see schematic illustration in Fig. 1A) [6, 8]. N-VEGF overlaps with IRES A and therefore the deletion of N-VEGF will affect only this IRES but not IRES B. It was expected that VEGF expression under hypoxia should not be severely affected by this deletion as shown hereafter. The CRISPR-Cas9 system was used with two sgRNAs, which target sequences near the 5' and 3' ends of N-VEGF (gRNA 1 and 4, respectively). Briefly, a two steps protocol was utilized to generate NIH3T3 cells with biallelic deletion of the N-VEGF. First, N-VEGF was replaced by mCherry reporter cassette flanked by VLoxP sites. Second, fluorescent cell clones were transduced with VCre encoding retroviral vector resulting in NIH3T3 clones with deleted N-VEGF (see schematic illustration in Fig. S3, and Materials and methods for details). Out of four clones, two such double-resistant clones harboring the biallelic N-VEGF replacement cassette were further verified by genomic PCR (Fig. S4 and Fig. S5). DNA sequencing was performed on a N-VEGF deleted clone that was further used in this study. To evaluate the success of our genomic deletion strategy and to verify that only N-VEGF expression and not VEGF was affected, cells were harvested before and following hypoxia and RNA was extracted. L-VEGF mRNA expression was induced only in NIH3T3 cell-line and not in the N-VEGF deleted counterpart clone, designated hereafter as ΔN-VEGF cells (Fig. 4A, left chart). Unlike L-VEGF, VEGF is induced in both cell types, except that the basal level of VEGF in the deleted cells is about 50% lower, but the fold of induction is similar. Furthermore, similar results were obtained by analysing cytoplasmic and nuclear protein extracts from these two cell types using Western blot analyses with polyclonal antibodies directed against either VEGF or N-VEGF (Fig. 4B). It is clear that N-VEGF is induced by hypoxia only in NIH3T3 cells and not in ΔN-VEGF cells. In NIH3T3 under normoxia N-VEGF is found in cytoplasmic fractions and following hypoxia it is confined to nuclear fractions (Fig. 4B, upper figure). It is also clear that VEGF is induced to a similar level following hypoxia in both cell types, regardless of N-VEGF deletion, and is confined only to cytoplasmic fractions (Fig. 4B, lower panel). This data shows that the deletion of N-VEGF, which also ablated IRES A, had no significant effect on the expression level of VEGF. Lastly, Ponceau S membrane staining and Western blot analyses were performed to show that similar amounts of proteins were loaded on the gels and that the cytoplasmic and nuclear soluble proteins fractions were not cross contaminated during the purification procedure as seen in supplemental Fig. S6. Next, immunostaining of these two cell types with antibodies directed against N-VEGF also demonstrate that

N-VEGF shuttles to the nuclei of NIH3T3 cells only upon hypoxia and is not detected in the counterpart deleted cells (Fig. 4C). Furthermore, both Western blot and Immunostaining analyses show that NIH3T3 cells have basal low level of VEGF expression as expected from a cell line that is maintained for many years since its initial isolation. Taken together, the NIH3T3 ΔN-VEGF cells exhibit no expression of N-VEGF but are still induced by hypoxia to express VEGF.

Differential gene expression profile between NIH3T3 and ΔN-VEGF cells following hypoxia

To show the effect of N-VEGF deletion on the transcriptome landscape and to unravel its nuclear role, RNA-Seq analysis was performed on the two cell types before and following hypoxia (see Materials and methods). A heatmap comparing the gene expression patterns before and following hypoxia in NIH3T3 and ΔN-VEGF cells is presented in Fig. 5A. In addition, a qualitative representation of this heatmap of gene expression in the two cell types only following hypoxia is presented in Fig. 5B. The gene are grouped according to expression pattern similarity or dissimilarity between the two cell types (G1-G6, indicated Fig. 5). The number of genes in each group is indicated within the right column of Fig. 5B. Similar expression pattern in both cell types of either induced or repressed genes are represented in groups G1 and G6, respectively. Inverse expression pattern between the two cell types following hypoxia is presented in groups G3 and G4. Lastly, genes that exhibited no change in expression pattern in ΔN-VEGF cells that were either upregulated or downregulated in NIH3T3 cells following hypoxia are represented in group G2 and G5, respectively. The annotation of all these gene groups following hypoxia or under normoxia were performed using Metascape as elaborated above [18] and are listed in Table S2, G1-G6. It is clear that under hypoxia, ΔN-VEGF cells are inducing 1530 genes (group G1) that overlap with the 2040 genes (groups G1+G2) that are induced in NIH3T3 cells (Fig. 5). Further, 1188 shared genes were downregulated in ΔN-VEGF cells (group G6) out of the 2084 genes (groups G6, G5 and G4) that were downregulated in NIH3T3 in response to hypoxia (Fig. 5). The annotations of up and downregulated genes are shown in Fig. 6A and 6D, respectively. Taken together, close to 70% of the analyzed genes exhibited similar expression pattern (induced (G1) or repressed (G6)) in the two cell types in response to hypoxia. Thus, deletion of N-VEGF led to a partial yet significant change in gene expression profile following hypoxia. The interesting groups are those that are composed of genes that exhibited inverse expression pattern between these two cell types (Fig. 5, G3 and G4,). The third group (G3) consist of 86 genes that were upregulated in NIH3T3 cells but were downregulated in ΔN-VEGF counterpart cells (Figs. 5, and Table S2, G3). Interestingly, the annotated groups are exclusively associated with cell cycle as well as DNA replication, repair, and maintenance (Fig. 6B). The fourth group (G4) includes 128 genes that were

upregulated in ΔN-VEGF cells and downregulated in NIH3T3 following hypoxia (Figs. 5 and Table S2, G4). The most significant annotation groups are extracellular matrix (ECM) organization and interactions with receptors as well as PI3K-Akt signaling pathway members (Fig. 6C). These annotated genes involved in cell-ECM interactions were implicated in the regulation of cell survival and proliferation in response to hypoxia [20]. The last two groups, G2 and G5 represent genes whose expression were not changed in ΔN-VEGF cells and were either upregulated or downregulated in response to hypoxia in NIH3T3 cells, respectively. We consider these groups as less relevant to N-VEGF activity as evident by the intensity of the differential expression representation in Fig. 5A, and therefore will not be discussed further. The annotations for these groups are presented in Fig. S7 and table S2 (G2 and G5), altogether, 31% of the analyzed genes exhibited differential expression. However, the most interesting gene groups are G3 and G4 that exhibited inverse expression pattern in ΔN-VEGF cells in comparison to NIH3T3 cells and represent only 5% of the analyzed genes. Taken together, the contribution of N-VEGF to cellular processes in cells under stress is best manifested in the ΔN-VEGF cells. The interplay between these two gene groups exhibiting inverse expression pattern during hypoxia is elaborated under Discussion. Finally, the changes in the transcriptome profile of NIH3T3 cells in response to hypoxia significantly overlap with changes observed in many cell types subjected to hypoxia as evidenced by meta-analysis of hypoxic transcriptomes from public databases (Table S2) [21].

Numbers on right lower corner of each bar graph represent the group number in blue and the genes number in the group in black.

Comparative gene expression pattern in cells expressing nuclear N-VEGF independent of hypoxia and cells following hypoxia

Although VEGF is a key player in response to hypoxia, there are many other factors involved including VEGF-B, VEGF-C, Basic FGF 2, Platelet Derived Growth Factor 2 [16]. These growth factors elicit an overlapping or a redundant angiogenic response with VEGF in response to hypoxia. It should be noted that the mRNA for this differential expression study was extracted 16 hrs following hypoxia, thus, it is possible that some early activated genes were already downregulated. The notable change in the transcriptome profile between NIH3T3 and ΔN-VEGF cells following hypoxia does not allow identification of early genes in these stress-mediated signaling cascades. Therefore, we performed a comparative gene expression analysis in cells following hypoxia and cells expressing nuclear N-VEGF regardless of hypoxia. As sown above, hypoxia independent mobilization of N-VEGF resulted in the identification of the 155 genes (123 upregulated and 32 downregulated). We expected that genes that will

exhibit similar expression pattern in both cell types will highlight once again the role of N-VEGF in hypoxia and cells maintenance during stress. Further, we expected that early hypoxia responding genes will exhibit differential expression pattern in cells expressing nuclear N-VEGF regardless of hypoxia. A qualitative heatmap was generated that shows the similarities and dissimilarities in the expression pattern of these 155 genes between these two cell types treatments, dox vs hypoxia (Fig.7A). The four annotated groups are shown in Fig. 7, panels B-E. The first annotated groups include 51 genes that were induced and 14 genes that were downregulated in both NIH3T3 following hypoxia and NLS-N-VEGF cells (Fig. 7B and Fig. 7E, respectively). Altogether, 42% of the genes exhibited similar expression pattern. The annotated groups of upregulated genes that exhibited similar expression, are grouped into three main categories: initiation of angiogenic pathways, cell response to stress by regulating apoptosis and the major category, maintenance of cellular structure during hypoxic stress (Fig. 7B). The genes that were downregulated in NLS-N-VEGF cells as well as in NIH3T3 cells following hypoxia are associated with catabolic process of proteins (Fig. 7E) [22]. Taken together, this analysis underscores the role of N-VEGF in these pathways in response to hypoxia. Further, 90 genes (58%) exhibited differential expression. (Fig. 7C and D). In this group include 72 genes that were upregulated in NLS-N-VEGF cells following dox that in NIH3T3 cells following hypoxia were either downregulated or their expression was not affected (Fig. 7C). The major annotated groups are associated with regulation of cell morphology, cell migration and angiogenesis. Lastly,18 genes were upregulated or not changed in NIH3T3 cells following hypoxia and were downregulated in NLS-N-VEGF cells following dox treatment (Fig. 7D). The statistical significance of the annotated groups is low due to the small number of genes. However, the major annotations are associated with negative regulation of proteins translation and modification along with cell proliferation, representing typical responses to hypoxia [1]. Taken together, this focused gene profile expression analysis highlights the role of N-VEGF in initiating part of the cellular response to hypoxia as will be elaborated onwards. Further, the genes that exhibit differential expression in NLS-N-VEGF cells may represent early hypoxia response genes that were already down or up regulated in NIH3T3 cells after 16 hrs of hypoxia.

Comparative gene expression pattern in cells expressing nuclear N-VEGF independent of hypoxia and N-VEGF deleted cells following hypoxia

As elaborated above, hypoxia independent mobilization of N-VEGF allowed the identification of the 155 genes that are directly affected by this nuclear isoform (123 upregulated and 32 downregulated). Therefore, we expected that some of these early hypoxia responding genes will exhibit inverse expression

pattern in N-VEGF deleted cells highlighting the role of N-VEGF in the conservation of cells during hypoxia. Accordingly, a qualitative heatmap was generated that shows the similarities and dissimilarities in the expression pattern of these 155 genes between these two cell types (Fig. 8A). It is clear that following hypoxia or dox treatment (ΔN-VEGF cells and NLS-N-VEGF cells, respectively) 55 genes were upregulated, and 17 genes were downregulated in both cell types (46%). The annotation groups of these genes are shown in Fig. 8A and E, respectively. However, the expression pattern of 54% of the genes exhibit opposite expression pattern in ΔN-VEGF cells (Fig. 8C-D). The annotated groups of genes include cellular morphogenesis, cholesterol biosynthesis, cytoskeleton organization, cell adhesion, cellular responses to oxidative stress, and negative regulation of apoptosis. Taken together, the data further highlights the unique regulatory role of this nuclear isoform of VEGF in cells maintenance and survival during stress.

N-VEGF elicits survival response in hypoxic cells.

Six genes encoding for, Aqp1, Msn, Sgk1, Src, Nrp1, and Pik3c2a, which are associated with negative regulation of apoptotic signaling pathway [23-28], were upregulated by nuclear expression of N-VEGF and downregulated in ΔN-VEGF cells following hypoxia. This suggests that N-VEGF deleted cells might be more susceptible to stress signal such as hypoxia. To demonstrate the fragility of ΔN-VEGF cells in comparison to their counterpart undeleted cells, we compared their apoptotic index following three different, yet similar, stress signals. This includes hypoxia, $CoCl_2$ [29], and serum deprivation [30] all resulting in induced VEGF mRNA expression. The effect of endoplasmic reticulum stress (ER) [31], which did not lead to VEGF induction in NIH3T3 cells (data not shown), was also tested. It is clear from Fig. 9 that all those VEGF inducing stress signals led to enhanced and statistically significant apoptosis of ΔN-VEGF cells in comparison to NIH3T3 cells (Fig. 9A, B and C, respectively). On the other hand, ER stress did not elicit a significant change in the apoptotic index between N-VEGF deleted cells in comparison to their WT counterpart cells (Fig. 9D). Taken together, N-VEGF is involved in mediating anti-apoptotic state in the stressed cells to overcome the harsh conditions until oxygen or blood supplies are improved.

The Src-Ras pathway mediates some of the anti-apoptotic response to hypoxia

Among the anti-apoptotic annotated gene products that caught our attention is Src, that mediates signaling cascades such as angiogenesis, cell proliferation and more (see Fig. S8 for schematic illustration) [25]. Our data suggests that downregulation of the Src gene may lead to cells fragility under hypoxia. To test this hypothesis, NIH3T3 cells and ΔN-VEGF counterpart cells were subjected to hypoxia in the presence

or absence of the Src inhibitor Dasatinib, a Src multi-kinase inhibitor [32]. It is clear that NIH3T3 cells exposed to Dasatinib (1μM) under hypoxia exhibited reduced viability, significantly elevated cytotoxicity, and enhanced apoptosis in comparison to ΔN-VEGF cells that already exhibit reduced Src expression as a result of N-VEGF deletion (Fig. 10, upper row). Since Src is at the checkpoint between several signaling pathways that are initiated by activated Src, two additional inhibitors, Lonafarnib and GSK690693, that inhibit Ras and AKT, respectively, were tested [33, 34]. Ras is downstream of Src and AKT is downstream of PI3K that can be activated by Src and Receptor Tyrosine Kinase (RTK) (Fig. S8, highlighted in black). Ras, harboring GTPase domain, is downstream of Src in the signaling pathway leading to cell proliferation and angiogenesis [25]. It is also engaged in pro- or anti-apoptotic regulation, depending on the cell type. Respectively, Ras protects epithelial cells from apoptosis [35]. It is clear from Fig. 10 (middle row) that exposure of NIH3T3 cells to hypoxia and Lonafarnib (15μm) resulted in an increased cell death, cytotoxicity, and a significant increase in apoptosis. Like the Src inhibitor, the Ras inhibitor was much less potent in affecting the viability, toxicity, and apoptotic index of ΔN-VEGF cells under hypoxia. Last, AKT, a Serine/Threonine Kinase, is involved in cell survival and is a downstream effector of the PI3K signaling pathway, that can be activated by RTK directly and/or via activated Src [36]. Unlike the Src and the Ras inhibitors, it is clear from Fig. 10 (bottom row) that there was no significant differential effect of GSK690693 (25μM) on the viability, cytotoxicity, and apoptotic index, between NIH3T3 cells and the counterpart ΔN-VEGF cells following hypoxia. The choice of optimal concentration of the inhibitors is detailed under Materials and methods and Fig. S9.

Taken together, using specific cell singling inhibitors on one hand and genomic deletion of N-VEGF on the other hand, our results highlight the role of the Src-Ras pathway in protecting hypoxic NIH3T3 cells from cell death. During hypoxia, this pathway is activated, whereas, the AKT pathway does not seem to have a cell survival role in NIH3T3 cells during hypoxia.

Discussion

L-VEGF and its proteolytic product N-VEGF (formerly termed uORF) were identified twenty years ago. Yet, its role during hypoxia is not clear. Here we provide evidence demonstrating that N-VEGF potentiates maintenance of angiogenesis along with cell survival circuits. Hypoxia is a severe cellular stress that lead to cellular injury and cell death. In response to hypoxia, cells induce the expression of gene sets that are involved in pathways aimed at minimizing cellular damage and enable survival. Among the many cellular

rescue pathways activated in response to hypoxia are genes involved in the initiation of angiogenesis, in inhibiting apoptotic pathways, and in the maintenance of cellular structure [37]. This was demonstrated in many cell types subjected to hypoxia by meta-analysis of hypoxic transcriptomes from public databases [21]. Respectively, our data demonstrate typical changes in the transcriptome profile in response to hypoxia of NIH3T3 cell line used in this study (Table S2). Further, nuclear localization of N-VEGF in various normal as well as cancer cell lines and tissues was also reported as detailed above [10-14]. Therefore, the results presented here represent the genuine potential of N-VEGF. To our surprise, hypoxia-independent mobilization of N-VEGF to cells nuclei, led to differential expression of 155 unique genes that are associated with these signaling pathways. Signature genes mediating angiogenesis such as Hif1α, Adgrg1, Itgav, Nrp, Flna, Pik3c2a, and more were upregulated by NLS-N-VEGF following dox-mediated induction (Fig. 2, purple columns, and Table S1) [38]. Similarly, genes such as Sh3rf1 [39], Lrrk2 [40] and Src that are associated with anti-apoptotic pathways were also induced by NLS-N-VEGF (Fig. 2, brown columns, and Table S1). Lastly, NLS-N-VEGF also induced the expression of genes that are associated with the maintenance of the cellular structural integrity such as Cav2 [41], Lamc2 [42], Cfl2 [41], Rock2 [43], and more. Remarkably, many of these genes are also induced directly or indirectly by Hif1α, a major hypoxia induced mediator of gene expression [44], that is also induced by NLS-N-VEGF. Comparison of the expression pattern of the 155 genes that are either induced or downregulated following hypoxia-independent nuclear mobilization of N-VEGF with the expression signature of hypoxia-induced genes in NIH3T3 cells (Fig. 7), highlights the pivotal role of N-VEGF in the initiation of cellular responses to hypoxia. The identification of N-VEGF immediate target genes that elicit these angiogenesis and cell survival circuits is a matter of future research.

To elucidate the role of N-VEGF, we specifically knocked-out L-VEGF using CRISPR-Cas9. To our surprise, interfering with the expression of just N-VEGF led to a notable change in gene expression patterns 16 hrs following the onset of hypoxia (Figs. 5 and 6). This differential gene expression profile between NIH3T3 cell-line and its N-VEGF deleted counterpart highlights the role of this non-canonical VEGF isoform of VEGF in cellular response to hypoxia (Fig. 5 and Table S2). As expected, the induction of VEGF expression by hypoxia in the N-VEGF knock-out cells was similar to that of NIH3T3 cells (Fig. 4B). Furthermore, the fact that many genes were still upregulated (1530) or downregulated (1188) in both cell types in response to hypoxia (66% compared to NIH3T3 cells) indicates that a significant response to hypoxia is still occurring in the deleted cells independently of N-VEGF (Fig.5 G1 and G6, respectively). However, other groups of genes displayed an inverse expression pattern in response to hypoxia in the

knock-out cells in comparison to wild-type NIH3T3 cells (Fig. 5 G3-G4 and table S2), indicating that N-VEGF has an independent and necessary part in the regulation of the response to hypoxic stress. In that respect, the downregulated 86 genes (Fig. 5 and Fig. 6B, Table S2, G2), indicate that the nuclear localization of N-VEGF has a direct impact on specific nuclear processes in the stressed cells, such as cell cycle regulation, DNA replication and maintenance. Indeed, the cross talk between hypoxia and the cell cycle, and the impact of hypoxia on DNA repair and genome integrity are well documented [37, 45, 46]. Interestingly, several genes that are associated with DNA repair and maintenance as well as chromosome stability such as, Chk1, BRCA1, BRCA2, RAD51, RAD51B, NBS, FANCD2, RAD54, MSH2, MSH6, MYH, MTH1, failed to be upregulated in response to hypoxia in N-VEGF deleted cells in comparison with NIH3T3 cells (for review see [45]). Conversely, the expression of the 128 genes of group G4, that were induced by hypoxia following the deletion of N-VEGF, led to the induction of compensatory pathways involved in cellular maintenance such as ECM organization, structure (focal adhesions), and interaction with receptors. Anchorage-dependent cells, such as endothelial cells, undergo apoptosis when detached from underlying extracellular matrix [47]. ECM is an essential modulator of cell survival and behavior that influences tissue organization. We have shown that N-VEGF deleted cells are more prone to apoptosis in response to hypoxia, cell starvation, and inhibition of oxygen transport by $CoCl_2$ (Fig. 9). It is most likely that in response to increased apoptosis cells are more apoptotic. Hence, the survival balance in N-VEGF deleted cells is shifting towards increasing expression of genes essential for ECM organization and structure that have anti-apoptotic effect [41]. The fact that many genes associated with DNA replication and repair as well as cell cycle are downregulated in the N-VEGF deleted cells in comparison to NIH3T3 under normoxia suggests a possible role of N-VEGF as a key checkpoint factor in mediating genome stability during stress [46].

The deletion of N-VEGF resulted in a notable change in the expression profile of genes in response to hypoxia in comparison to the parental NIH3T3 cells. We decided to focus on the expression pattern of the 155 genes that exhibited differential expression pattern following stress-independent nuclear mobilization of N-VEGF as detailed above. We predicted that some of these genes are not directly affected by N-VEGF but are rather a part of a signaling cascade response. To identify genes that are more likely to be directly activated or repressed by N-VEGF, we scrutinized genes that exhibit inverse expression pattern in N-VEGF deleted cells (Fig. 8C and 8D). The annotated groups of genes that display inverse expression pattern between NLS-N-VEGF and ΔN-VEGF cells can be narrowed to maintenance of cellular structure, cellular membranes, and extra cellular organization together with cellular response to

stress and prevention of apoptosis. A small group of genes including Aqp1, Msn, Sgk1, Src, Nrp1, and Pik3c2a were annotated as negative regulation of apoptotic signaling pathway and attracted our attention, [23-28]. These genes were upregulated by nuclear expression of N-VEGF and downregulated in ΔN-VEGF cells. Interestingly, almost all of these genes, Aqp1, Sgk1, Src, Nrp1, and Pik3c2a, are involved in angiogenesis signaling as well, [48-52]. This data further supports the role of N-VEGF in preventing cell death on one hand and promoting angiogenesis on the other hand to enable cells to endure the hypoxic stress.

N-VEGF deleted cells were significantly more apoptotic following stress signals (Fig. 9) and the Src, Ras, and AKT genes were downregulated. This highlights the role of these genes in cell survival, proliferation, motility, and angiogenesis pathways following hypoxia [53]. Taken together, it suggested that NIH3T3 cells and N-VEGF deleted cells would exhibit similar fragility during hypoxia if these genes will be inhibited. Our data show that following hypoxia, inhibition of Src and Ras but not AKT elicited elevated cell cytotoxicity and enhanced apoptosis (Fig. 10). This suggests, that during hypoxia, the Src-Ras pathway, promoting angiogenesis that eventually leads to cell survival, is more dominant in NIH3T3 cells as previously shown for colon cancer cells [53]. Our data add new molecular insight to the pros and cons of using Src and Ras inhibitors in colon cancer (for review see [54]). Further, N-VEGF elicits the expression of two angiogenesis key genes, VEGF, (isoform 120 and 164) and Hif1α (Fig. 3A). A naive hypothesis awaiting further experiments is that in response to hypoxia, N-VEGF leads to autocrine loop by further inducing Hif1α that in response leads to the induction of VEGF that signals back via VEGF Receptor 2 leading to cell survival by the activation of Src-Ras pathway [50].

Interestingly, a single polymorphism in the 5'-UTR of the VEGF gene within the coding region of L-VEGF/N-VEGF was associated with diabetic retinopathy in type 2 diabetes [55]. This C(−634)G polymorphism was manifested in an increased levels of VEGF thus suggesting a novel genetic risk factor for diabetic retinopathy. Further, using the genomAD browser [56], which tests for the presence of rare mutations in the general population, the genomic region of the L-VEGF\N-VEGF exhibits high concentration of stop codons. In contrast, the number of rare mutations that affect the VEGF (VEGF-A) gene is slightly lower than statistically expected indicating that there is a weak negative selection for mutations in VEGF. Considering that most of these mutations actually occur in the L-VEGF\N-VEGF genomic region implies that loss of L-VEGF\N-VEGF expression is not as detrimental as loss of VEGF, which leads to early embryonic lethality [57, 58]. Accordingly, deletion of N-VEGF resulted in more fragile but not complete apoptotic cells and its role during embryogenesis is a matter of future research.

Deletion of N-VEGF resulted in knockout of L-VEGF as well. The biological roles of L-VEGF are not clear. It is suggested that L-VEGF may serve as a reservoir for shorter isoforms when the availability of canonical VEGF short isoforms is limited. Further, L-VEGF was implicated in ALS, in the development of macular retinal thickness, in an increased risk of breast cancer aggressiveness, and in gastric as well as prostate cancer. This is due to a genomic polymorphism resulting in IRES B dysfunction, which eventually leads to a reduced translation of L-VEGF from a CUG codon (reviewed in [1], see schematic illustration in Fig. 1A). In light of the data presented here, the role of N-VEGF, a proteolytic product of L-VEGF, should be revisited in these cases. Yet, the possibility that some of the genes that exhibited differential expression are due to the lack of L-VEGF, cannot be completely excluded. However, the importance of N-VEGF in mediating cellular response to hypoxia is manifested by the hypoxia-independent nuclear mobilization of N-VEGF as demonstrated here.

The molecular mechanisms by which N-VEGF is executing these activities are not clear and are a matter of future studies. The significant change in transcriptome profile between N-VEGF deleted cells and the counterpart parental cells, suggests that it acts as a direct inducer of key genes essential for cell cycle, cell maintenance, and survival.

Materials and methods

Cell lines

NIH3T3 (mouse embryo fibroblast) and 293FT (human embryonal kidney) were obtained from ATCC, Manassas, VA (CRL-1658 and CRL-3216, respectively). These cell lines were maintained in DMEM supplemented with 10% fetal calf serum (FCS), amphotericin (2.5 μg/mL) and gentamycin sulfate (50 μg/mL, Biological Industries, Beit-Haemek, Israel).

Plasmid construction

Lentiviral vector, pLVX-Tet-One-Puro vector (Clontech, #631847), encoding for an engineered Tet activator and the corresponding inducible promoter, which is induced by doxycycline (dox, a derivative of tetracycline), was used. Using PCR a 180 aa N-VEGF containing also 5’ 6xHis-tag was generated, digested with the restriction enzymes EcoRI and AgeI, and cloned into pLVX-Tet-One-Puro vector termed here N-VEGF. Similarly, a DNA fragment harboring a 5’ 6xHis-tag, an effective NLS, taken from the Cas9 gene and 180aa of N-VEGF was generated by PCR and digested with the restriction enzymes EcoRI and AgeI, and cloned into this vector thus termed NLS-N-VEGF. These clones’ integrity was verified by DNA sequencing.

Lentiviral production

$4x10^6$ 293FT cells were seeded in 10cm tissue culture plate 24hrs prior to transfection. Five µg of lentiviral vector, 1 µg pMD.G and 4 µg psPAX2 were transfected using CalFectin, mammalian transfection reagent (SignaGen, Maryland, USA) according to manufacturer's instructions. Twenty-four hrs post-transfection medium was changed with 7 ml of fresh medium. Forty-eight hrs post-transfection viral supernatant was collected, filtered using 0.2µm syringe-filter and aliquots were flash-freezed using liquid nitrogen. The viral supernatant was stored at -80 ^{0}C for further use.

NIH3T3 infection

Twenty-four hrs prior to infection, 2.5x 10^5 cells were seeded in a 12 well tissue plate with 0.5 ml of medium. Then, 0.5 ml of viral supernatant and 8 µg/ml of polybrene were added to each well. The cells were incubated at 37^{0}C in 5% CO_2 incubator. Twenty-four hrs post-transfection, the cells were split 1:2 into 6 well tissue culture plates. Stably infected cells were selected with Puromycin (3µg/ml) for 48 hrs post-infection and resistant cells were harvested 96 hrs later.

Nuclear and cytoplasmic fractionation

NIH3T3 cells were trypsinized (2x10cm plates) and washed twice with ice cold PBS and lysed on ice for 15min in 100µl of cytoplasmic lysis buffer (10mM HEPES pH 7.4, 10mM KCl, 0.01mM EDTA, 0.1mM EGTA, 2mM DTT, 5mM Na¬2VO4, 0.1% NP40 and cOmplete, EDTA-free protease inhibitor cocktail (Sigma-Aldrich). Nuclei were pelleted using benchtop microfuge (6,000rpm for 2 min) and the supernatant containing the cytoplasmic fraction removed to which Urea and SDS were added to a final concentration of 2M and 2%, respectively. The samples were denatured by boiling for 5 min. The nuclei were then washed twice in 1ml of cytoplasmic lysis buffer to remove any cytoplasmic contaminant, and re-sedimented. Subsequently, the nuclei were lysed in 100µl of denaturing lysis buffer (2% SDS, 2M urea, 8% sucrose, 1mM NaF, and 5mM Na¬2VO4). Genomic DNA was sheared by passage through a Qiashredder column (Qiagen, Crawley, UK) in a benchtop microfuge (6,000rpm for 2 min) and denatured by boiling for 5 min.

SDS-PAGE and Western blotting

SDS-PAGE and Western blotting were preformed using Bio-Rad Mini-protein apparatus. Gel was prepared and blotted, and reacted with antibodies exactly as previously described [13]. The primary antibody used was Rabbit polyclonal αORF (N-VEGF), made in our laboratory, that was affinity purified against 5'UTRORF of VEGF (1:500 dilution in TBST+2.5% non-fat dried milk-powder (Carnation)). The

primary antibody was incubated for 3 hrs at R.T or O.N. at 4^0C. Secondary antibody, HRP anti-rabbit (1:10,000 dilution in TBST+2.5% non-fat dried milk-powder) was incubated for 1-2 hrs. Bands were visualized using ECL2 Western Blotting kit (Thermo Scientific, Waltham, MA).

To demonstrate even loading of protein samples, membranes were stained, prior to membranes blocking, with Ponceau-S (Sigma-Aldrich) according to the manufacturer's instructions and exactly as described before [59]. The purity of cytoplasmic and nuclear soluble protein extracts was determined by Western blot. Membranes were striped from anti N-VEGF or VEGF polyclonal antibodies and following re-blocking reacted with primary antibodies directed against Lactate Dehydrogenase (anti-LDH) (Abcam, cat #ab47010,1:300) and secondary antibodies anti-goat (1:10,000), to test nuclear extract purity. Subsequently the membrane was striped once more from bound antibodies, re-blocked, and reacted with antibodies directed against Histone H3 acetyl K27 (αH3K27ac) primary antibody (Abcam, #ab4729, 1:500) and secondary antibodies, anti-rabbit (1:10,000) to test cytoplasmic extract purity.

Immunofluorescence staining and microscopy

NIH3T3 cells, transfected with a vector driving the expression of either N-VEGF or NLS-N-VEGF, were plated in 24 wells plates containing microscope coverslips 0.13 mm. Some of the samples were treated with 1 µg/ml dox for 48 hrs. After additional 24 hrs, the cells were either not treated or subjected to hypoxia for additional 16 hrs. Cells were fixed with 4% PFA for 15 min at room temperature, washed two times with PBST, permeabilized with 0.1% Triton X-100 for 15 min and washed three times. Cells were then blocked with 5% normal goat serum in TBST for 1 hrs and subjected to staining with primary antibodies directed against N-VEGF (1:100 dilution in blocking solution) for O.N at 4 ^{0}C in a humidified chamber with very gentle swirling. Finally, the coverslips were washed four times with PBS. Slides were subsequently reacted with fluorescent secondary antibodies Alexaflour 488 goat anti rabbit (H+L) (1:1000 dilution in blocking solution) for 1 hr in the dark at RT. Following incubation, the slides were washed three times with PBS and reacted with DAPI and Fluromount-G for nuclei staining. Immunostained cells were visualized under Cell Observer-Zeiss inverted fluorescence microscope, magnification x20.

Real-time RT-PCR

The primers used for real-time PCR were designed using PrimerExpress™ software (Applied Biosystems; see Supplemental Table S3). 800 ng total RNA were reverse transcribed to cDNA using High-Capacity cDNA Reverse Transcriptase kit (Ambion) according to manufacturer's instructions. cDNA was amplified with two primers for each gene using Power SYBR Green PCR Master Mix (Applied Biosystems, USA)

and Real-time PCR analysis was performed using QuantStudio 12K Flex (Applied Biosystems by Life technology, USA), according to manufacturer's instructions. Gene expression was normalized to GAPDH mRNA expression. The data is presented as the relative expression of the gene of interest compared with GAPDH. The mRNA expression trend of genes mentioned in this publication (up, down or unchanged) that were determined by RNA-seq, were all validated by independent real time RT-PCR.

RNA-seq

RNA samples concentration and integrity were measured using Qubit (ThermoFisher) and TapeStation (Agilent), respectively. Libraries for sequencing were prepared using the TruSeq RNA Library Prep Kit v2 (Illumina) according to manufacturer's instructions. Libraries were sequenced on Illumina NextSeq 550 instrument with 80 bps single-read. The number of reads ranged from 54,915,873 to 38,372,655 per sample. Library quality control was conducted using FASTQC, version 0.11.5. Sequences were trimmed by quality using trim galore and aligned to Mus musculus genome build – GRCm38.p6 with release 94 annotation file using Tophat2, version 2.1.0 (uses Bowtie2 version 2.2.6). Raw gene expression levels were counted by HTseq-count, version 0.6.1. All downstream analyses were conducted in R with DESeq2 [60] as follows: raw data were filtered by independent filtering. Count normalization was performed by DESeq2 default. To identify differentially expressed genes differing between two conditions we used the Wald test, as implemented in DESeq2.

Heatmaps were plotted using R pheatmap package. For the heatmap normalized counts were scaled by row and the genes were ordered as specified in the figure legends.

All RNA sequencing data were deposited to the Gene Expression Omnibus (GEO) with accession numbers GSE178297 and GSE178298.

CRISPR/Cas9-mediated deletion of N-VEGF

The strategy for generating N-VEGF deleted cells is shown in Fig. S3. sgRNAs from the 5′ and 3′ ends of the 180 aa long N-VEGF were designed using the chopchop online tool [61], and highly scored sgRNAs were chosen (sgRNA 1–6). Each sgRNA was phosphorylated, annealed, and cloned to lentiGuide-Puro (addgene no. 52963), which was previously digested with BsmbI. In order to create gRNAs with sticky ends complementary to BsmbI digestion product, "CACC" and "AAAC" were added to 5′ end of the designed 20-bps sgRNA in the forward and reverse oligomers, respectively. In order to verify the efficiency and specificity of the sgRNAs, a T7 endonuclease assay was performed on NIH3T3 cells and the cleavage efficiency was analyzed using TapeStation (Agilent). Two gRNAs (1 and 4) were found to specifically targeted the ORF: gRNA1 target-site PCR amplicon (500 bps) was cleaved to 300 and 200 bp

fragments, and gRNA4 target-site PCR amplicon (461 bp) was cleaved into 329 and 132 bp fragments (data not shown). Briefly, a two steps protocol was utilized to generate NIH3T3 cells with biallelic deletion of the ORF. To get biallelic clones with reporter cassette insertion with high probability, cells were transfected with the two gRNAs and Cas9 encoding vector and two donor DNA segments (with different selectable markers, Puromycin and Hygromycin) and cultivated for 2 weeks. Single clones, resistant for the two antibiotics and containing mCherry reporter gene instead of the N-VEGF sequence, were picked and the 5′ and 3′ junctions were assayed by PCR (Fig. S4). Four Clones harboring the biallelic N-VEGF replacement cassette were further verified by DNA sequencing and taken for further study. For "clean" deletion of the N-VEGF two clones were transduced with pMSCV-VCre encoding retroviral vector [62] to remove the reporter\selection cassettes (Fig. S3). Three days later, non-fluorescent cells were harvested following two cycles of FACS sorting. N-VEGF deletion was verified by PCR and by DNA sequence analysis.

Flow cytometry

Flow cytometry sorting was performed using BD FACSAria-IIIu cell sorter (BD Bioscience), and data was analyzed using Flowing Software 2 (Cell Imaging Core, Turku Centre for Biotechnology). Unstained WT NIH3T3 cells were used as negative control and NIH3T3 cells containing mCherry reporter gene were used as positive control.

Hypoxia treatment

Hypoxic cultures were maintained in a hypoxia chamber (<0.2% O_2) for 16 hrs at 37°C in humidified 95% N_2/5% CO_2, and normoxic cultures were maintained in 95% air/5% CO_2 for similar duration.

ApoTox-Glo™Triplex assay

BD BioCoat Poly-D-Lysine 96-well plates with black sides and clear bottoms were used to run the ApoTox-Glo™ Triplex Assay (Promega). Cells were trypsinized and removed from their culture flasks and diluted to 24,000 cells/ml and 100µl of each sample was added to each well. Viability and Cytotoxicity reagents from the kit were prepared according to manufacturer's instructions, added to a 96-well plates, and the plates was incubated at 37°C for 1 hr. After incubation, plates were analyzed for fluorescence as defined in the protocol using a Spark® multimode microplate reader by Tecan. The caspase reagents were then added to the plates and the plates were incubated at RT for an additional 1 hr. Luminescence was then measured.

Treatment with Src, Ras, and AKT inhibitors

NIH3T3 and the corresponding ΔN-VEGF cells were grown for 24 hrs under normoxia in the absence or the presence of various concentrations of Dasatinib (0.25, 0.5, 1,2 μM [63]), Lonafarnib (20, 30, 50,100 μM [64]) and GSK690693 (20, 25, 30, 50 μM [65]), inhibitors of Src, Ras and AKT, respectively. All were purchased from Sigma-Aldrich catalogue numbers CDS023389, SML1457, and SML0428, respectively. The effect on the viability of both cell types was evaluated by Trypan Blue staining assays. The inhibitors concentrations that exhibited a reduction of about 20% in cell's viability in both cell types under normoxia were chosen (see Fig. S9). Accordingly, NIH3T3 and ΔN-VEGF cells were tested under normoxia or subjected to hypoxia for 24 hrs in the presence or the absence of the 1μM Dasatinib, 15μM Lonafarnib, and 25μM GSK690693. Viability, cytotoxicity, and apoptosis were determined using the ApoTox-GloTM Triplex Assays as detailed above.

Cobalt chloride and Tunicamycin treatments

Cobalt chloride (Spectrum) was added to a final concentration of 550 μM to N-VEGF NIH3T3 and the counterpart part ΔN-VEGF cell cultures. The live and dead cells were counted using trypan blue staining after 4, 6, 8 and 17 hrs of treatment. Next, the ApoTox-Glo™Triplex assay was used to test the viability, cytotoxicity, and apoptosis of the cells as detailed above.

Tunicamycin (Sigma) was added to a final concentration of 0.5 μg/ml to N-VEGF NIH3T3 and the counterpart part ΔN-VEGF cell cultures. The live and dead cells were counted using trypan blue staining after 5 hrs of treatment. Then the ApoTox-Glo™Triplex assay was used to test the viability, cytotoxicity, and apoptosis of the cells.

Statistical analysis

Each experiment was conducted at least three times in triplicates unless otherwise stated. Values are presented as means±AvDev. Except for Fig. 10, the data was compared by unpaired two-tailed Student's t-test; p-values <0.05 (*), <0.01(**) or <0.001 (***) were considered as statistically significant, as indicated in the appropriate figure. The statistical significance of the multicomponent data in Fig. 10 was determined in two steps. First, the effect of the inhibitors in each combination of cell types and assays before and following hypoxia was determined using unequal variances t-test. The p-values were corrected for multiple hypotheses testing using the Benjamini-Hochberg False Discovery Rate procedure with alpha<0.05. Second, to further compare the effects of cell type and stress in each assay, the difference between inhibitor and control were calculated for each combination of inhibitor, cell type, stress and assay in each biological replicate and Two-way ANOVA was performed on the differences with cell type and stress as main factors. The ANOVA was followed by post-hoc analysis of all possible contrasts using

Tukey's honestly significant difference, which controls for multiple comparisons. Contrasts with p-values <0.05 are considered significant. The statistical analyses were performed using the R language and environment for statistical computing and graphics.

Acknowledgements

We are grateful to the Gellman-Lasser Fund for Medical & Biomedical Research and innovation (grant No. 907679) to B.Z.L, and to the Technion's Genome Center and the Russell Berrie Nanotechnology Institute for their support. We are also deeply grateful to Prof. Gera Neufeld, Faculty of Medicine, Prof. Yuval Shoham, Faculty of Biotechnology and Food engineering and Dr. Nitsan Fourier, the genomic centre, Technion, for their input and critical reading of the manuscript. The initial construction of the Tet-On Lenti-vectors by Mrs Tania Vorobyov, research assistant, is acknowledged. B.Z.L. is an incumbent of the Lily and Silvian Marcus Chair in Life Sciences, Technion.

References

1. Arcondeguy T, Lacazette E, Millevoi S, Prats H, Touriol C. VEGF-A mRNA processing, stability and translation: a paradigm for intricate regulation of gene expression at the post-transcriptional level. Nucleic Acids Res. 2013;41(17):7997-8010. doi: 10.1093/nar/gkt539. PubMed PMID: 23851566; PubMed Central PMCID: PMCPMC3783158.
2. Apte RS, Chen DS, Ferrara N. VEGF in Signaling and Disease: Beyond Discovery and Development. Cell. 2019;176(6):1248-64. Epub 2019/03/09. doi: 10.1016/j.cell.2019.01.021. PubMed PMID: 30849371; PubMed Central PMCID: PMCPMC6410740.
3. Neufeld G, Cohen T, Gitay-Goren H, Poltorak Z, Tessler S, Sharon R, et al. Similarities and differences between the vascular endothelial growth factor (VEGF) splice variants. Cancer Metastasis Rev. 1996;15:153-8.
4. Ferrara N, Houck KA, Jakeman LB, Winer J, Leung WD. The vascular endothelial growth factor family of polypeptides. J Cellular Biochem. 1991;47:211-8.
5. Levy NS, Chung S, Furneaux H, Levy AP. Hypoxic stabilization of vascular endothelial growth factor mRNA by the RNA-binding protein HuR. J Biol Chem. 1998;273:6417-23.

6. Akiri G, Nahari D, Finkelstein Y, Le SY, Elroy-Stein O, Levi BZ. Regulation of vascular endothelial growth factor (VEGF) expression is mediated by internal initiation of translation and alternative initiation of transcription. Oncogene. 1998;17:227-36.

7. Huez I, L C, Audigier S, Gensac MC, Prats AC, Prats H. Two Independent Internal Ribosome Entry Sites Are Involved in Translation Initiation of Vascular Endothelial Growth Factor mRNA. Mol Cell Biol. 1998;18:6178-90.

8. Stein I, Itin A, Einat P, Skaliter R, Grossman Z, Keshet E. Translation of vascular endothelial growth factor mRNA by internal ribosome entry: implications for translation under hypoxia. Mol Cell Biol. 1998;18(6):3112-9.

9. Kraggerud SM, Sandvik JA, Pettersen EO. Regulation of protein synthesis in human cells exposed to extreme hypoxia. Anticancer Res. 1995;15:683-6.

10. Meiron M, Anunu R, Scheinman EJ, Hashmueli S, Levi BZ. New isoforms of VEGF are translated from alternative initiation CUG codons located in its 5'UTR. Biochem Biophys Res Commun. 2001;282(4):1053-60.

11. Tee MK, Jaffe RB. A precursor form of vascular endothelial growth factor arises by initiation from an upstream in-frame CUG codon. Biochem J. 2001;359(Pt 1):219-26.

12. Huez I, Bornes S, Bresson D, Creancier L, Prats H. New vascular endothelial growth factor isoform generated by internal ribosome entry site-driven CUG translation initiation. Mol Endocrinol. 2001;15(12):2197-210.

13. Rosenbaum-Dekel Y, Fuchs A, Yakirevich E, Azriel A, Mazareb S, Resnick MB, et al. Nuclear localization of long-VEGF is associated with hypoxia and tumor angiogenesis. Biochem Biophys Res Commun. 2005;332(1):271-8. doi: 10.1016/j.bbrc.2005.04.123. PubMed PMID: 15896327.

14. Bastide A, Karaa Z, Bornes S, Hieblot C, Lacazette E, Prats H, et al. An upstream open reading frame within an IRES controls expression of a specific VEGF-A isoform. Nucleic Acids Res. 2008;36(7):2434-45. doi: 10.1093/nar/gkn093. PubMed PMID: 18304943; PubMed Central PMCID: PMCPMC2367723.

15. Shih SC, Claffey KP. Hypoxia-mediated regulation of gene expression in mammalian cells. Int J Exp Pathol. 1998;79(6):347-57. Epub 1999/05/13. doi: 10.1046/j.1365-2613.1998.00088.x. PubMed PMID: 10319016; PubMed Central PMCID: PMCPMC3220374.

16. Hickey MM, Simon MC. Regulation of angiogenesis by hypoxia and hypoxia-inducible factors. Curr Top Dev Biol. 2006;76:217-57. Epub 2006/11/23. doi: 10.1016/S0070-2153(06)76007-0. PubMed PMID: 17118268.

17. Gossen M, Freundlieb S, Bender G, Muller G, Hillen W, Bujard H. Transcriptional activation by tetracyclines in mammalian cells. Science. 1995;268(5218):1766-9. PubMed PMID: 7792603.

18. Zhou Y, Zhou B, Pache L, Chang M, Khodabakhshi AH, Tanaseichuk O, et al. Metascape provides a biologist-oriented resource for the analysis of systems-level datasets. Nature communications. 2019;10(1):1523. Epub 2019/04/05. doi: 10.1038/s41467-019-09234-6. PubMed PMID: 30944313; PubMed Central PMCID: PMCPMC6447622.

19. Schneider CA, Rasband WS, Eliceiri KW. NIH Image to ImageJ: 25 years of image analysis. Nat Methods. 2012;9(7):671-5. Epub 2012/08/30. doi: 10.1038/nmeth.2089. PubMed PMID: 22930834; PubMed Central PMCID: PMCPMC5554542.

20. Clark EA, Brugge JS. Integrins and signal transduction pathways: the road taken. Science. 1995;268(5208):233-9. Epub 1995/04/14. doi: 10.1126/science.7716514. PubMed PMID: 7716514.

21. Bono H, Hirota K. Meta-Analysis of Hypoxic Transcriptomes from Public Databases. Biomedicines. 2020;8(1). Epub 2020/01/16. doi: 10.3390/biomedicines8010010. PubMed PMID: 31936636; PubMed Central PMCID: PMCPMC7168238.

22. Frezza C, Zheng L, Tennant DA, Papkovsky DB, Hedley BA, Kalna G, et al. Metabolic profiling of hypoxic cells revealed a catabolic signature required for cell survival. PLoS One. 2011;6(9):e24411. Epub 2011/09/14. doi: 10.1371/journal.pone.0024411. PubMed PMID: 21912692; PubMed Central PMCID: PMCPMC3166325.

23. Thompson MA, Edmonds MD, Liang S, McClintock-Treep S, Wang X, Li S, et al. miR-31 and miR-17-5p levels change during transformation of follicular lymphoma. Hum Pathol. 2016;50:118-26. Epub 2016/03/22. doi: 10.1016/j.humpath.2015.11.011. PubMed PMID: 26997445; PubMed Central PMCID: PMCPMC4804154.

24. Chao LM, Sun W, Chen H, Liu BY, Li PF, Zhao DW. MicroRNA-31 inhibits osteosarcoma cell proliferation, migration and invasion by targeting PIK3C2A. Eur Rev Med Pharmacol Sci. 2018;22(21):7205-13. Epub 2018/11/24. doi: 10.26355/eurrev_201811_16254. PubMed PMID: 30468462.

25. Abu-Ghazaleh R, Kabir J, Jia H, Lobo M, Zachary I. Src mediates stimulation by vascular endothelial growth factor of the phosphorylation of focal adhesion kinase at tyrosine 861, and migration

and anti-apoptosis in endothelial cells. Biochem J. 2001;360(Pt 1):255-64. Epub 2001/11/07. doi: 10.1042/0264-6021:3600255. PubMed PMID: 11696015; PubMed Central PMCID: PMCPMC1222225.

26. Yamazato Y, Shiozaki A, Ichikawa D, Kosuga T, Shoda K, Arita T, et al. Aquaporin 1 suppresses apoptosis and affects prognosis in esophageal squamous cell carcinoma. Oncotarget. 2018;9(52):29957-74. Epub 2018/07/26. doi: 10.18632/oncotarget.25722. PubMed PMID: 30042826; PubMed Central PMCID: PMCPMC6057448.

27. Bai JA, Xu GF, Yan LJ, Zeng WW, Ji QQ, Wu JD, et al. SGK1 inhibits cellular apoptosis and promotes proliferation via the MEK/ERK/p53 pathway in colitis. World J Gastroenterol. 2015;21(20):6180-93. Epub 2015/06/03. doi: 10.3748/wjg.v21.i20.6180. PubMed PMID: 26034353; PubMed Central PMCID: PMCPMC4445095.

28. Han Z, Jiang G, Zhang Y, Xu J, Chen C, Zhang L, et al. Effects of RNA interference-mediated NRP-1 silencing on the proliferation and apoptosis of breast cancer cells. Mol Med Rep. 2015;12(1):513-9. Epub 2015/03/05. doi: 10.3892/mmr.2015.3405. PubMed PMID: 25738638.

29. Sandner P, Wolf K, Bergmair U, Gess B, Kurtz A. Hypoxia and cobalt stimulate vascular endothelial growth factor receptor gene expression in rats. Pflugers Arch. 1997;433:803-8.

30. Li Y, Zhang H, Xie M, Hu M, Ge S, Yang D, et al. Abundant expression of Dec1/stra13/sharp2 in colon carcinoma: its antagonizing role in serum deprivation-induced apoptosis and selective inhibition of procaspase activation. Biochem J. 2002;367(Pt 2):413-22. Epub 2002/07/18. doi: 10.1042/BJ20020514. PubMed PMID: 12119049; PubMed Central PMCID: PMCPMC1222902.

31. Bull VH, Thiede B. Proteome analysis of tunicamycin-induced ER stress. Electrophoresis. 2012;33(12):1814-23. Epub 2012/06/29. doi: 10.1002/elps.201100565. PubMed PMID: 22740470.

32. Roskoski R, Jr. Src protein-tyrosine kinase structure, mechanism, and small molecule inhibitors. Pharmacol Res. 2015;94:9-25. Epub 2015/02/11. doi: 10.1016/j.phrs.2015.01.003. PubMed PMID: 25662515.

33. Morgillo F, Lee HY. Lonafarnib in cancer therapy. Expert Opin Investig Drugs. 2006;15(6):709-19. Epub 2006/05/31. doi: 10.1517/13543784.15.6.709. PubMed PMID: 16732721.

34. Hers I, Vincent EE, Tavare JM. Akt signalling in health and disease. Cell Signal. 2011;23(10):1515-27. Epub 2011/05/31. doi: 10.1016/j.cellsig.2011.05.004. PubMed PMID: 21620960.

35. Downward J. Ras signalling and apoptosis. Curr Opin Genet Dev. 1998;8(1):49-54. Epub 1998/04/08. doi: 10.1016/s0959-437x(98)80061-0. PubMed PMID: 9529605.

36. Kennedy SG, Wagner AJ, Conzen SD, Jordan J, Bellacosa A, Tsichlis PN, et al. The PI 3-kinase/Akt signaling pathway delivers an anti-apoptotic signal. Genes Dev. 1997;11(6):701-13. Epub 1997/03/15. doi: 10.1101/gad.11.6.701. PubMed PMID: 9087425.

37. Bristow RG, Hill RP, Kaplan AR, Glazer PM. Hypoxia and metabolism. Hypoxia, DNA repair and genetic instability Impact of hypoxia on DNA repair and genome integrity. Nat Rev Cancer. 2008;8(3):180-92. Epub 2008/02/15. doi: 10.1038/nrc2344. PubMed PMID: 18273037.

38. Stelzer G, Rosen N, Plaschkes I, Zimmerman S, Twik M, Fishilevich S, et al. The GeneCards Suite: From Gene Data Mining to Disease Genome Sequence Analyses. Curr Protoc Bioinformatics. 2016;54:1 30 1-1 3. Epub 2016/06/21. doi: 10.1002/cpbi.5. PubMed PMID: 27322403.

39. Wilhelm M, Kukekov NV, Schmit TL, Biagas KV, Sproul AA, Gire S, et al. Sh3rf2/POSHER protein promotes cell survival by ring-mediated proteasomal degradation of the c-Jun N-terminal kinase scaffold POSH (Plenty of SH3s) protein. J Biol Chem. 2012;287(3):2247-56. Epub 2011/12/01. doi: 10.1074/jbc.M111.269431. PubMed PMID: 22128169; PubMed Central PMCID: PMCPMC3265902.

40. Bae YH, Joo H, Bae J, Hyeon SJ, Her S, Ko E, et al. Brain injury induces HIF-1alpha-dependent transcriptional activation of LRRK2 that exacerbates brain damage. Cell Death Dis. 2018;9(11):1125. Epub 2018/11/14. doi: 10.1038/s41419-018-1180-y. PubMed PMID: 30420654; PubMed Central PMCID: PMCPMC6232134.

41. Varela-Guruceaga M, Belaidi E, Lebeau L, Aka E, Andriantsitohaina R, Giorgetti-Peraldi S, et al. Intermittent Hypoxia Mediates Caveolae Disassembly That Parallels Insulin Resistance Development. Front Physiol. 2020;11:565486. PubMed PMID: 33324235.

42. Huang B, Xiao E, Huang M. MEK/ERK pathway is positively involved in hypoxia-induced vasculogenic mimicry formation in hepatocellular carcinoma which is regulated negatively by protein kinase A. Med Oncol. 2015;32(1):408. Epub 2014/12/10. doi: 10.1007/s12032-014-0408-7. PubMed PMID: 25487444.

43. Pandey P, Kumari S, Ali Z, Pasha MQ. Acute hypobaric hypoxia augments ROCK2 protein level and activity. Exp Lung Res. 2017;43(4-5):181-6. Epub 2017/06/29. doi: 10.1080/01902148.2017.1333174. PubMed PMID: 28657365.

44. Ferrara N, Gerber HP, LeCouter J. The biology of VEGF and its receptors. Nat Med. 2003;9(6):669-76. doi: 10.1038/nm0603-669. PubMed PMID: 12778165.

45. Semenza GL. Hypoxia. Cross talk between oxygen sensing and the cell cycle machinery. Am J Physiol Cell Physiol. 2011;301(3):C550-2. PubMed PMID: 21677261.

46. Kaplan AR, Glazer PM. Impact of hypoxia on DNA repair and genome integrity. Mutagenesis. 2020;35(1):61-8. PubMed PMID: 31282537.

47. Ruoslahti E, Reed JC. Anchorage dependence, integrins, and apoptosis. Cell. 1994;77(4):477-8. Epub 1994/05/20. doi: 10.1016/0092-8674(94)90209-7. PubMed PMID: 8187171.

48. Saadoun S, Papadopoulos MC, Hara-Chikuma M, Verkman AS. Impairment of angiogenesis and cell migration by targeted aquaporin-1 gene disruption. Nature. 2005;434(7034):786-92. Epub 2005/04/09. doi: 10.1038/nature03460. PubMed PMID: 15815633.

49. Lang F, Stournaras C, Zacharopoulou N, Voelkl J, Alesutan I. Serum- and glucocorticoid-inducible kinase 1 and the response to cell stress. Cell Stress. 2018;3(1):1-8. Epub 2019/06/22. doi: 10.15698/cst2019.01.170. PubMed PMID: 31225494; PubMed Central PMCID: PMCPMC6551677.

50. Summy JM, Gallick GE. Treatment for advanced tumors: SRC reclaims center stage. Clin Cancer Res. 2006;12(5):1398-401. Epub 2006/03/15. doi: 10.1158/1078-0432.CCR-05-2692. PubMed PMID: 16533761.

51. Neufeld G, Cohen T, Shraga N, Lange T, Kessler O, Herzog Y. The neuropilins: multifunctional semaphorin and VEGF receptors that modulate axon guidance and angiogenesis. Trends Cardiovasc Med. 2002;12(1):13-9. Epub 2002/02/14. doi: 10.1016/s1050-1738(01)00140-2. PubMed PMID: 11796239.

52. Margaria JP, Ratto E, Gozzelino L, Li H, Hirsch E. Class II PI3Ks at the Intersection between Signal Transduction and Membrane Trafficking. Biomolecules. 2019;9(3). Epub 2019/03/20. doi: 10.3390/biom9030104. PubMed PMID: 30884740; PubMed Central PMCID: PMCPMC6468456.

53. Zeng M, Kikuchi H, Pino MS, Chung DC. Hypoxia activates the K-ras proto-oncogene to stimulate angiogenesis and inhibit apoptosis in colon cancer cells. PLoS One. 2010;5(6):e10966. Epub 2010/06/10. doi: 10.1371/journal.pone.0010966. PubMed PMID: 20532039; PubMed Central PMCID: PMCPMC2881039.

54. Jin W. Regulation of Src Family Kinases during Colorectal Cancer Development and Its Clinical Implications. Cancers (Basel). 2020;12(5). Epub 2020/05/28. doi: 10.3390/cancers12051339. PubMed PMID: 32456226; PubMed Central PMCID: PMCPMC7281431.

55. Awata T, Inoue K, Kurihara S, Ohkubo T, Watanabe M, Inukai K, et al. A common polymorphism in the 5'-untranslated region of the VEGF gene is associated with diabetic retinopathy in type 2 diabetes. Diabetes. 2002;51(5):1635-9. Epub 2002/04/30. doi: 10.2337/diabetes.51.5.1635. PubMed PMID: 11978667.

56. Koch L. Exploring human genomic diversity with gnomAD. Nat Rev Genet. 2020;21(8):448. Epub 2020/06/04. doi: 10.1038/s41576-020-0255-7. PubMed PMID: 32488197.

57. Carmeliet P. VEGF as a key mediator of angiogenesis in cancer. Oncology. 2005;69 Suppl 3:4-10. Epub 2005/11/23. doi: 10.1159/000088478. PubMed PMID: 16301830.

58. Ferrara N, Carver-Moore K, Chen H, Dowd M, Lu L, O'Shea KS, et al. Heterozygous embryonic lethality induced by targeted inactivation of the VEGF gene. Nature. 1996;380:439-42.

59. Cohen H, Azriel A, Cohen T, Meraro D, Hashmueli S, Bech-Otschir D, et al. Interaction between interferon consensus sequence-binding protein and COP9/signalosome subunit CSN2 (Trip15). A possible link between interferon regulatory factor signaling and the COP9/signalosome. J Biol Chem. 2000;275(50):39081-9. Epub 2000/09/19. doi: 10.1074/jbc.M004900200. PubMed PMID: 10991940.

60. Love MI, Huber W, Anders S. Moderated estimation of fold change and dispersion for RNA-seq data with DESeq2. Genome Biol. 2014;15(12):550. Epub 2014/12/18. doi: 10.1186/s13059-014-0550-8. PubMed PMID: 25516281; PubMed Central PMCID: PMCPMC4302049.

61. Labun K, Montague TG, Krause M, Torres Cleuren YN, Tjeldnes H, Valen E. CHOPCHOP v3: expanding the CRISPR web toolbox beyond genome editing. Nucleic Acids Res. 2019;47(W1):W171-w4. Epub 2019/05/21. doi: 10.1093/nar/gkz365. PubMed PMID: 31106371; PubMed Central PMCID: PMCPMC6602426.

62. Suzuki E, Nakayama M. VCre/VloxP and SCre/SloxP: new site-specific recombination systems for genome engineering. Nucleic Acids Res. 2011;39(8):e49. Epub 2011/02/04. doi: 10.1093/nar/gkq1280. PubMed PMID: 21288882; PubMed Central PMCID: PMCPMC3082901.

63. Nautiyal J, Majumder P, Patel BB, Lee FY, Majumdar AP. Src inhibitor dasatinib inhibits growth of breast cancer cells by modulating EGFR signaling. Cancer Lett. 2009;283(2):143-51. Epub 2009/04/29. doi: 10.1016/j.canlet.2009.03.035. PubMed PMID: 19398150.

64. Smalley KS, Eisen TG. Farnesyl transferase inhibitor SCH66336 is cytostatic, pro-apoptotic and enhances chemosensitivity to cisplatin in melanoma cells. Int J Cancer. 2003;105(2):165-75. Epub 2003/04/04. doi: 10.1002/ijc.11064. PubMed PMID: 12673674.

65. Levy DS, Kahana JA, Kumar R. AKT inhibitor, GSK690693, induces growth inhibition and apoptosis in acute lymphoblastic leukemia cell lines. Blood. 2009;113(8):1723-9. Epub 2008/12/10. doi: 10.1182/blood-2008-02-137737. PubMed PMID: 19064730.

FIGURES

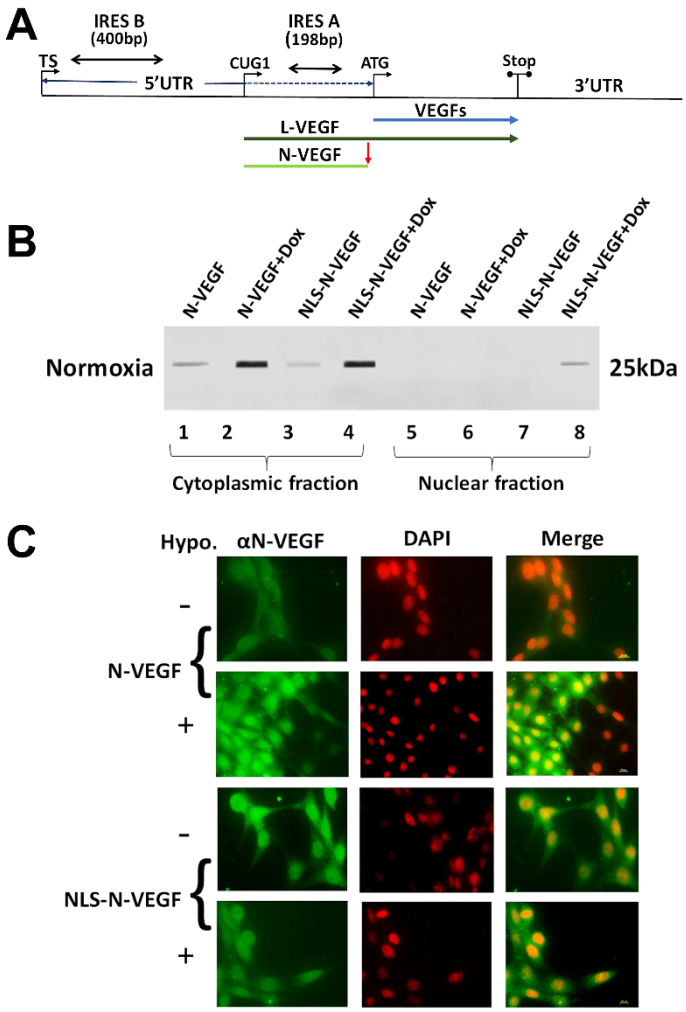

Fig. 1 N-VEGF is mobilized to cell's nuclei independent of hypoxia. (A) Schematic illustration of VEGF genomic organization and the translated products. TS-transcription start site. CUG1- L-VEGF translation start site, ATG-VEGF translation start site. Red arrow – estimated position of the proteolytic site of N-VEGF. The locations of IRES A and B are indicated by solid black arrows. The 5'UTR is indicated by a blue arrow, and when dashed its overlapped region with IRES. (B) NIH3T3 cells were transfected with pLVX-Tet-One-Puro vector harboring N-VEGF or NLS-N-VEGF. Forty-eight hours later, transfected cells were selected with puromycin and 96 hrs later, cells were harvested and used for Western blots and Immunofluorescence staining. Cells were treated or not treated with dox for 48 hrs. Subsequently, cytoplasmic and nuclear soluble proteins (as indicated in the figure) were isolated, loaded on SDS-Page gels, and subjected to Western blot analyses using antibodies against N-VEGF. (C) NIH3T3 cells were plated on microscope coverslips and subsequently infected with Lentiviral vectors driving the expression of N-VEGF or NLS-NVEGF in the presence of dox for 48 hrs. Cells were then subjected or not subjected to hypoxia, as indicated in the figure, for additional 16 hrs. Subsequently, Immunofluorescent staining with antibodies directed against N-VEGF and nuclear staining with DAPI were performed. The coverslips were visualized under fluorescent microscope (X20 magnification). For details see Materials and methods.

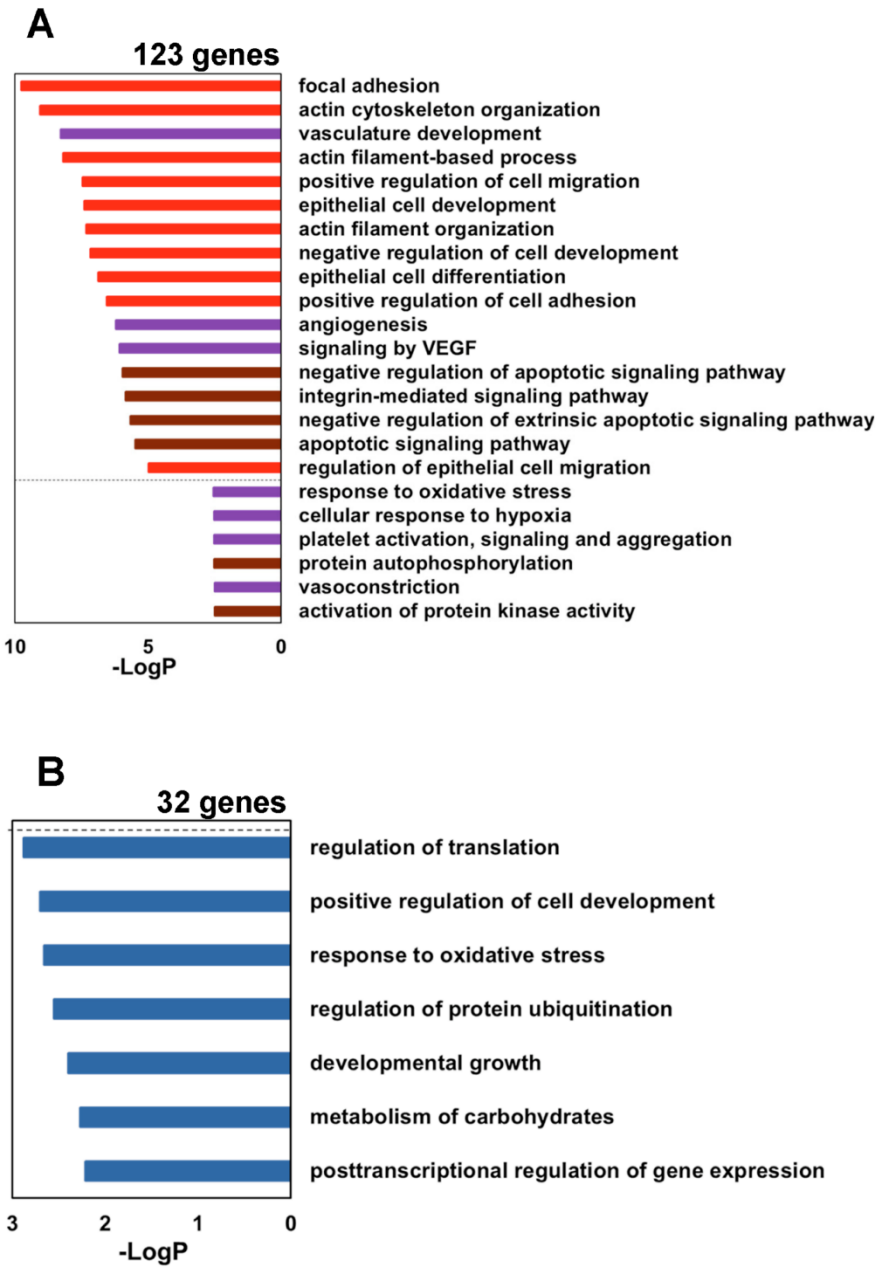

Fig. 2 Annotation and pathway analysis of the 155 differentially expressed genes following hypoxia independent nuclear mobilization of NLS-N-VEGF. The top gene ontology terms as determined by Metascape are presented. Database for Annotation Visualization and Integrated Differentially expressed genes were used as input gene list, and all murine genes were used as the background. Significant differential expressed genes with a log2 fold change ≥ 2 were analyzed for enriched biological processes using Metascape. The vertical axis represents the pathway category, and the horizontal axis (-LogP) represents the -Log10 (p-value) of the pathways. Greater –LogP scores indicate lower p-values hence stronger statistical significance. (A) The most significant annotations for upregulated genes. Annotated pathways were colored according to cellular function; purple bars, pathways supporting angiogenesis, brown bars, apoptotic signaling pathways, red bars, maintenance of cellular structure pathways. (B) The annotations for the downregulated genes.

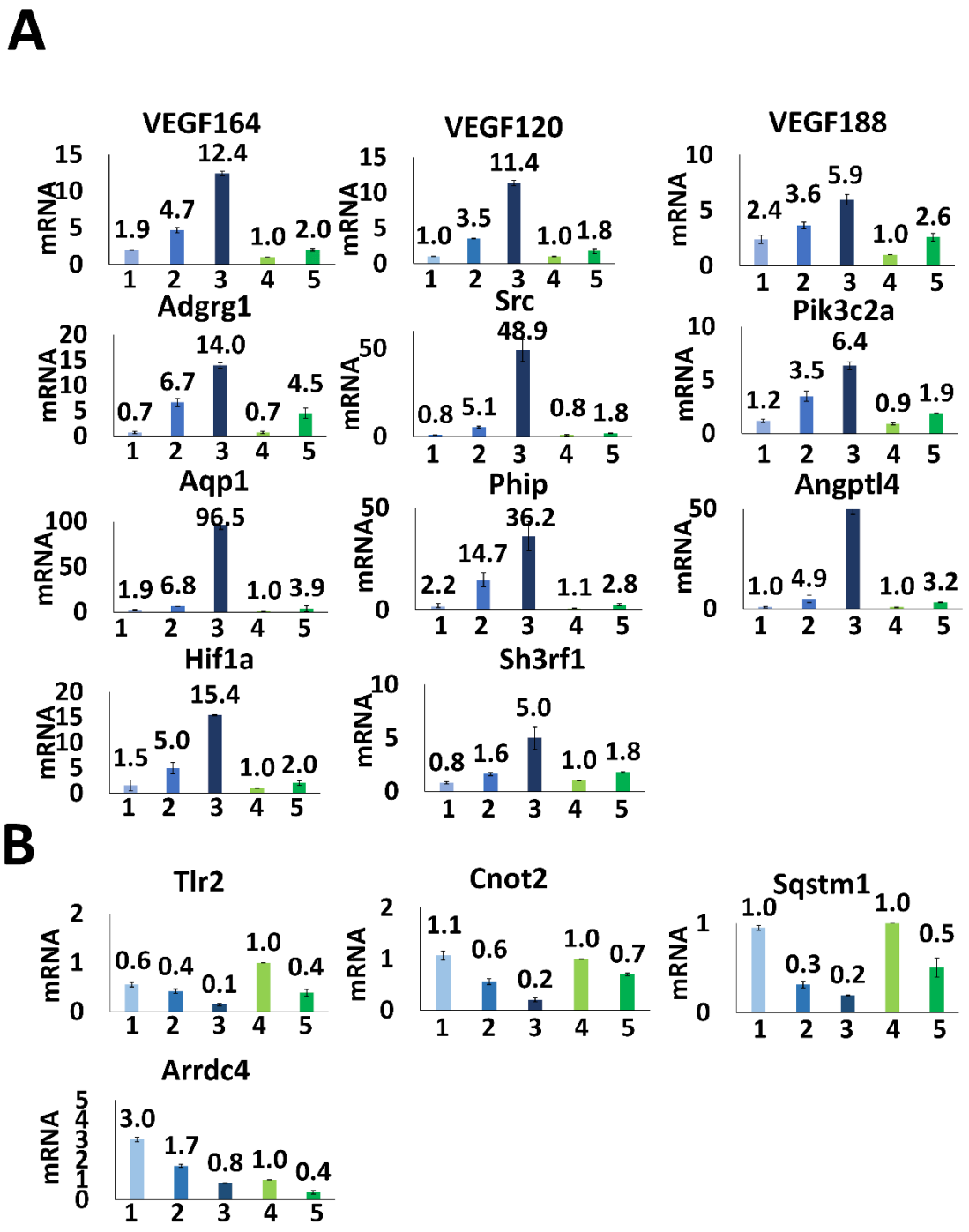

Fig. 3 Validation of the RNA-seq results. Real-time RT-qPCR analyses were performed on selected genes from each functional annotation group. The data is presented for NLS-L-VEGF before and following treatments with dox or dox combined with hypoxia; column 1 - light blue, column 2 - blue, and column 3 - dark blue, respectively). It is compared to control NIH3T3 cells before and following hypoxia; column 4 - light green and column 5 - dark green, respectively. (A) Selected upregulated genes. (B) Selected downregulated genes. Fold change in mRNA levels in triplicates from three independent experiments was determined. Values are mean± AVEDEV.

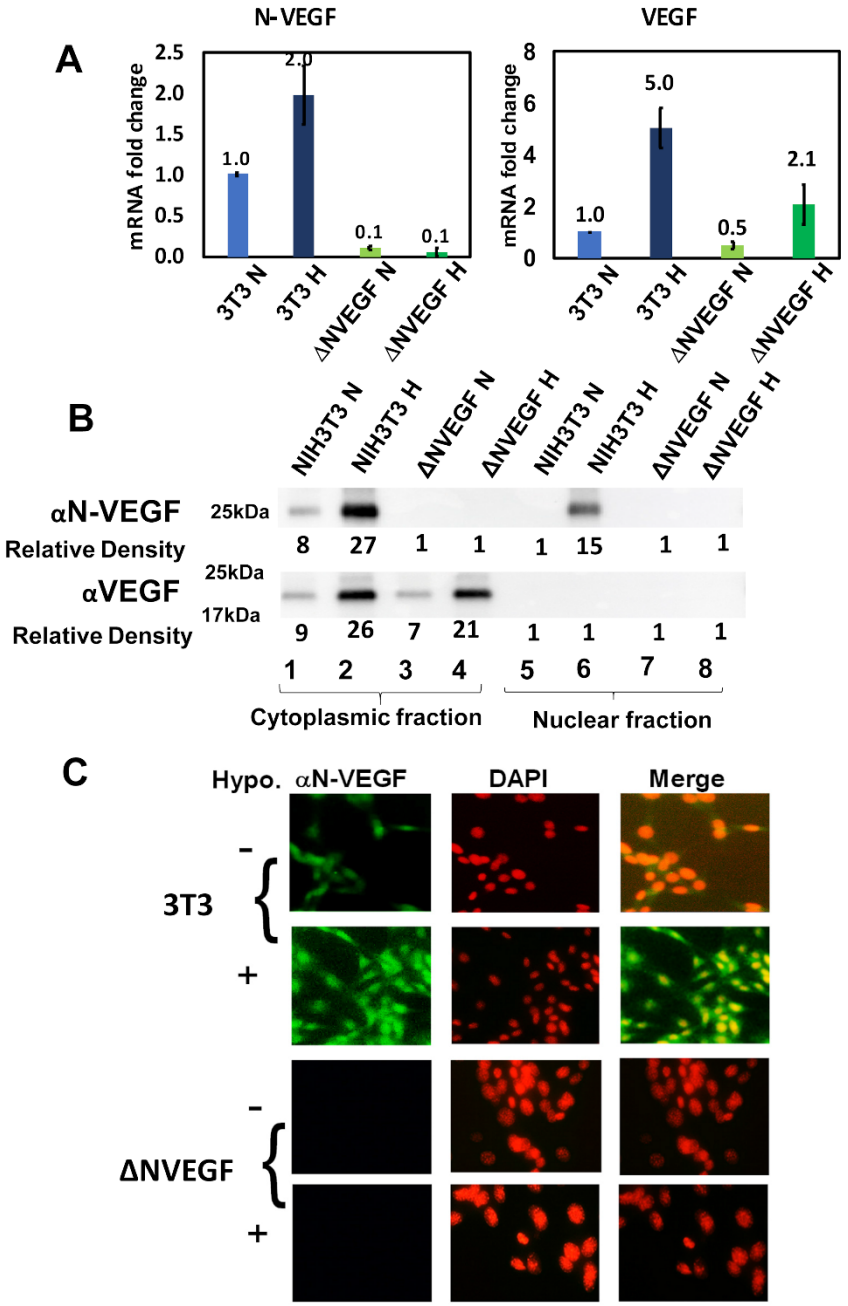

Fig. 4 NIH3T3 ΔN-VEGF cells still express VEGF following hypoxia. (A) NIH3T3 ΔN-VEGF cells (ΔNVEGF) and NIH3T3 (3T3) cells were harvested under normoxia (N) and following hypoxia (H) and RNA was extracted. The mRNA levels of N-VEGF and classical VEGFs were determined by Real-time RT-qPCR from three independent experiments. Values are mean ± AVEDEV (n=3), Student's t-test. (B) Western blot analyses with polyclonal antibodies directed against VEGF and N-VEGF were performed with cytoplasmic and nuclear soluble protein extracts from ΔN-VEGF (ΔNVEGF) and NIH3T3 (3T3) cells following normoxic (N) and hypoxic conditions (H). Numbers below lanes indicate the relative density of the band as determined by ImageJ software [65]. (C) NIH3T3 (3T3) and ΔN-VEGF (ΔNVEGF) cells were plated on microscope slides and were either not treated (N) or subjected to hypoxia (H). The cells were then fixed, permeabilized, blocked and subjected to immunostaining staining as detailed under Fig. 1.

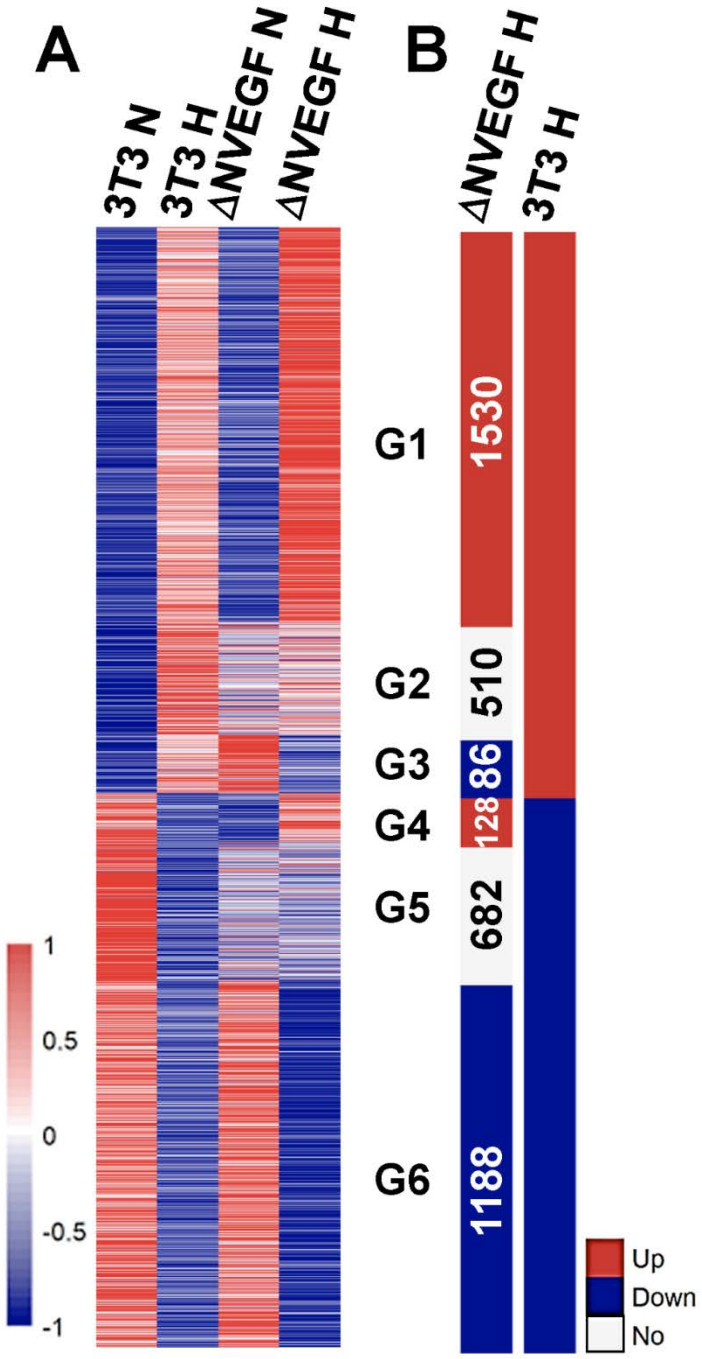

Fig. 5 Differential gene expression between NIH3T3 cells and their counterpart deleted cells under normoxia and following hypoxia. (A) a four columns heatmap is showing relative differential gene expression response between NIH3T3 cells (3T3) and ΔN-VEGF counterpart cells (ΔNVEGF) under normoxia (N) and following hypoxia (H) as detailed under Materials and methods. The genes are ordered by the direction of the differential (upregulated/downregulated) in NIH3T3 cells under normoxia. Expression level scale is shown on the left side lower corner. (B) The two columns represent a qualitative heatmap showing the direction of change in gene expression level in response to hypoxia in ΔN-VEGF cells (ΔNVEGF H) in comparison to NIH3T3 cell under normoxia (3T3 N). Six groups (G1-G6) of upregulated (red), downregulated (blue) or expression not changed (white) are denoted. The numbers in each group region within the left column in panel B represent the number of differential genes in each group.

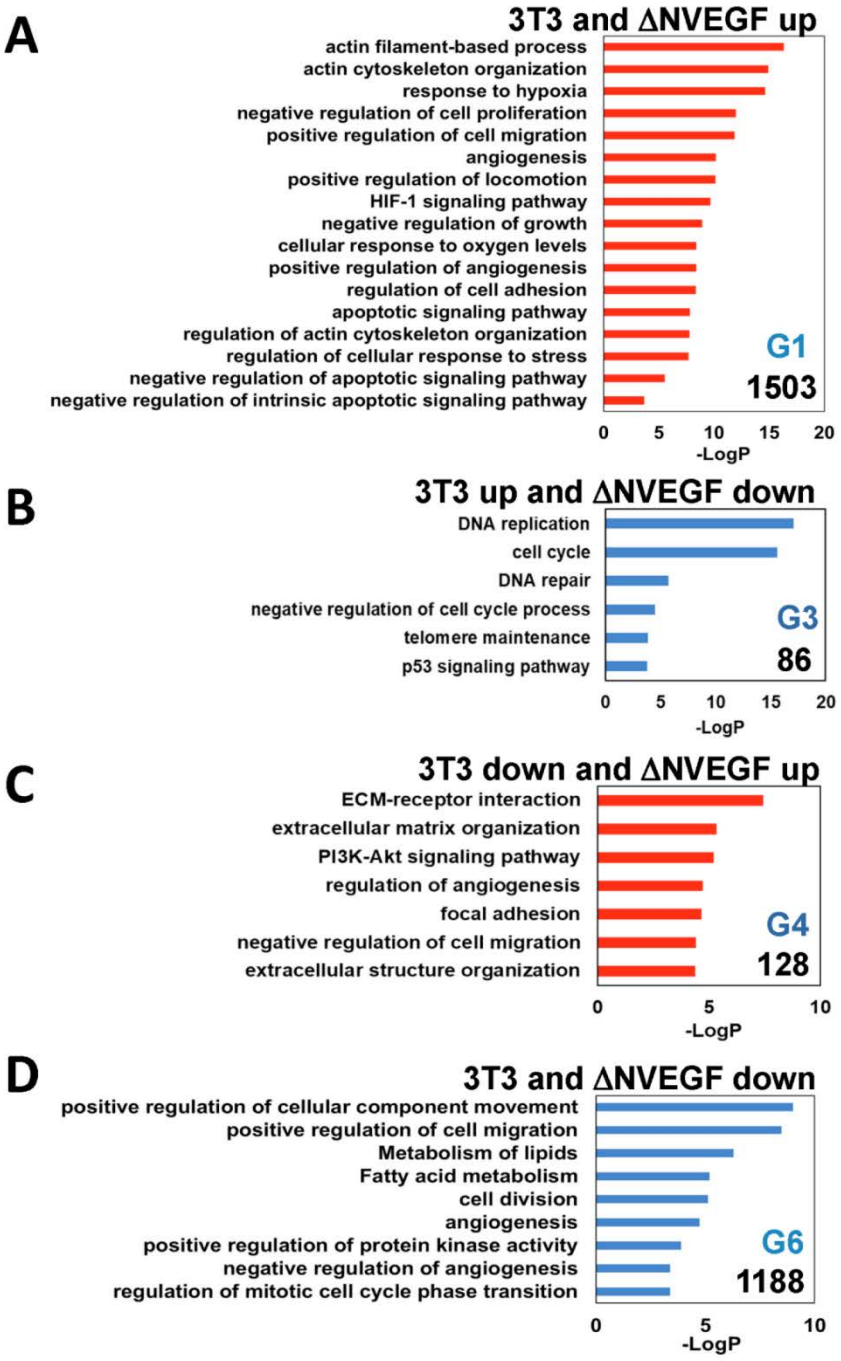

Fig. 6 Differential pathways annotation between up\down regulated genes in NIH3T3 cells and ΔN-VEGF cells following hypoxia. Annotation of the differential genes in groups G1, G3, G4 and G6 using Metascape is presented (panels A-D, respectively). (A) Red bars - annotated pathways for genes that were upregulated in both cell types following hypoxia (G1). (B) Blue bars - annotated pathways for genes that were downregulated in ΔN-VEGF cells and induced in NIHN3T3 cells following hypoxia (G3). (C) Red bars - annotated pathways for upregulated genes in ΔN-VEGF cells and downregulated in NIH3T3 cells following hypoxia (G4). (D) Blue bars - annotated pathways for genes that were downregulated in both cell types following hypoxia (G6). Numbers on right lower corner of each bar graph represent the group number in blue and the genes number in the group in black.

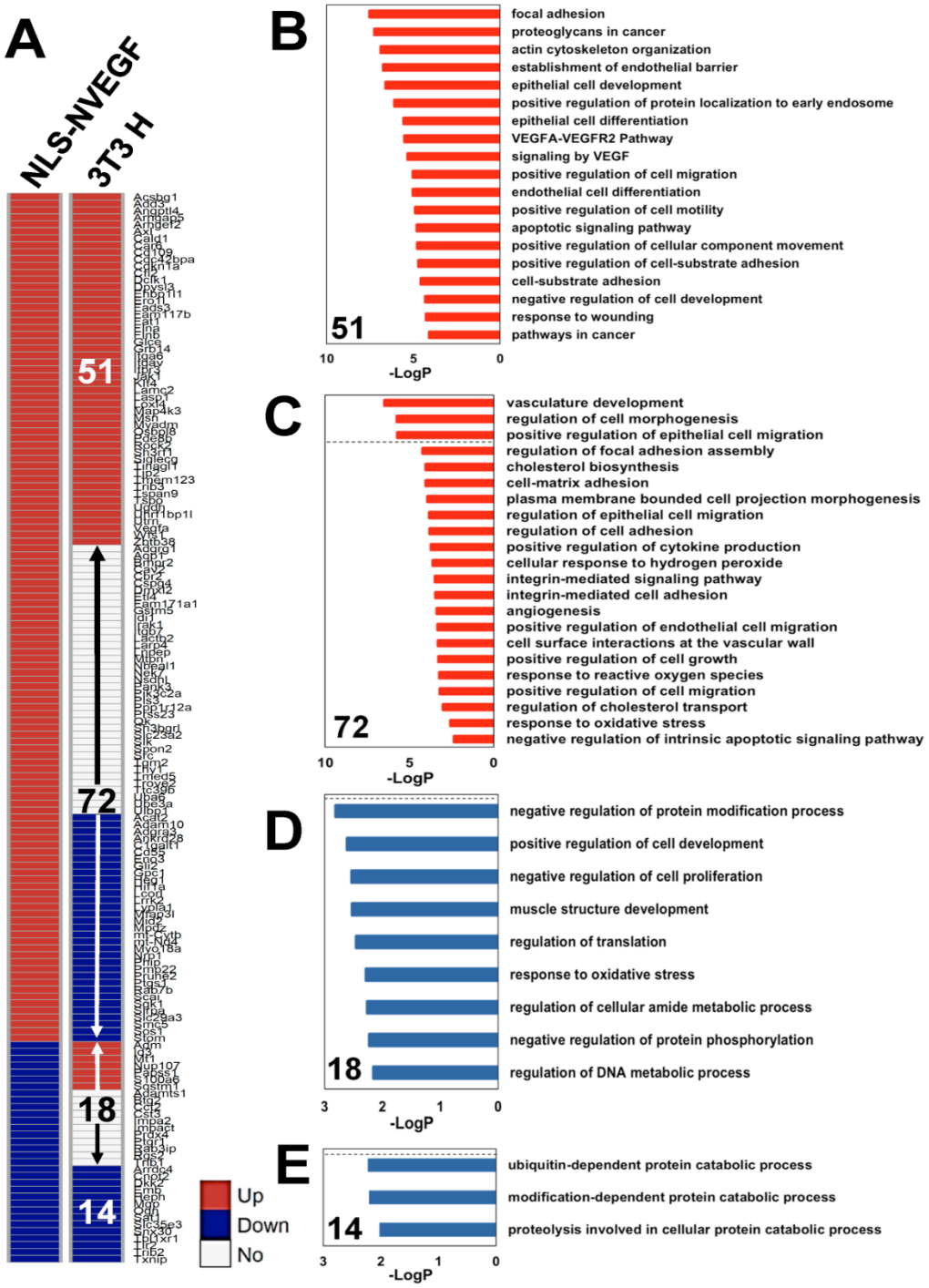

Fig. 7 Comparison between 155 genes that exhibited differential expression in NLS-N-VEGF cells and NIH3T3 cells following hypoxia. (A) The columns represent a qualitative heatmap showing the direction of change in gene expression level (up-red, down-blue, no change (no)-white) in NLS-N-VEGF cells following dox treatment (NLS-NVEGF, left column) in comparison to NIH3T3 cell under hypoxia (3T3 H, right column). The numbers within the right column represent the number of genes in each group that were annotated in panels B-E. (B) Annotation of genes (51) that were upregulated in both cell types. (C) annotation of genes (72) that were upregulated in NLS-N-VEGF cells following dox and not changed or downregulated in NIH3T3 cells. (D) annotation of genes (18) that were downregulated in NLS-N-VEGF cells following dox and upregulated or not changed in NIH3T3 cells. (E) Annotation of genes (14) that were downregulated in both cell types. Bars below dotted line represent less significant annotation groups.

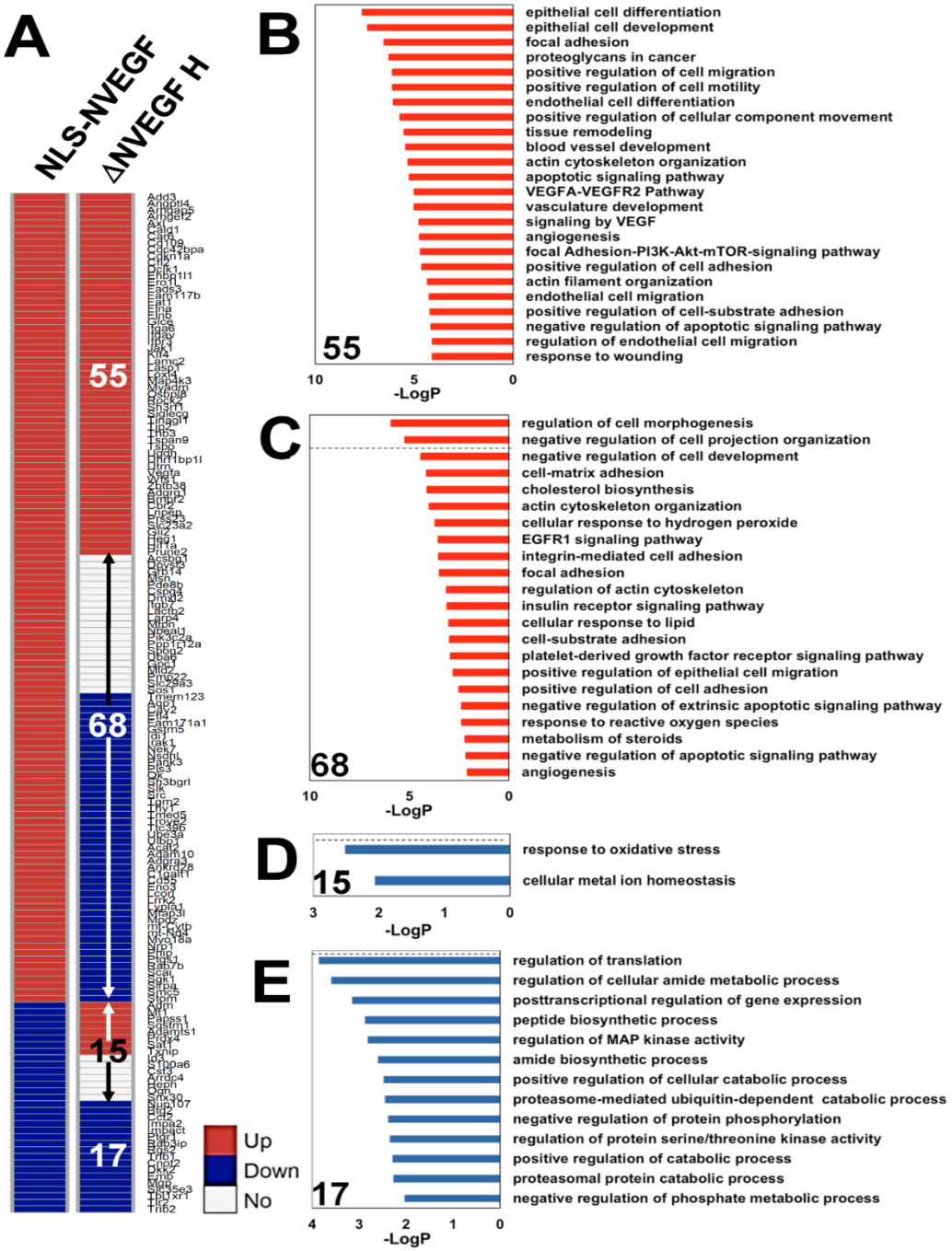

Fig. 8 Comparison between 155 genes that exhibited differential expression in NLS-N-VEGF cells and ΔN-VEGF cells following hypoxia. (A) The columns represent a qualitative heatmap showing the direction of change in gene expression level (up-red, down-blue, no-white) in NLS-N-VEGF cells following dox treatment (NLS-NVEGF, left column) in comparison to ΔN-VEGF cells under hypoxia (ΔNVGF H, right column). The numbers within the right columns represent the number of genes in each group that were annotated in panels B-E. (B) Annotation of genes (55) that were upregulated in both cell types. (C) annotation of genes (68) that were upregulated in NLS-N-VEGF cells following dox and not changed or downregulated in ΔN-VEGF cells. (D) annotation of genes (15) that were downregulated in NLS-N-VEGF cells following dox and upregulated or not changed in ΔN-VEGF cells. (E) Annotation of genes (17) that were downregulated in both cell types. Bars below dotted line represent less significant annotation groups.

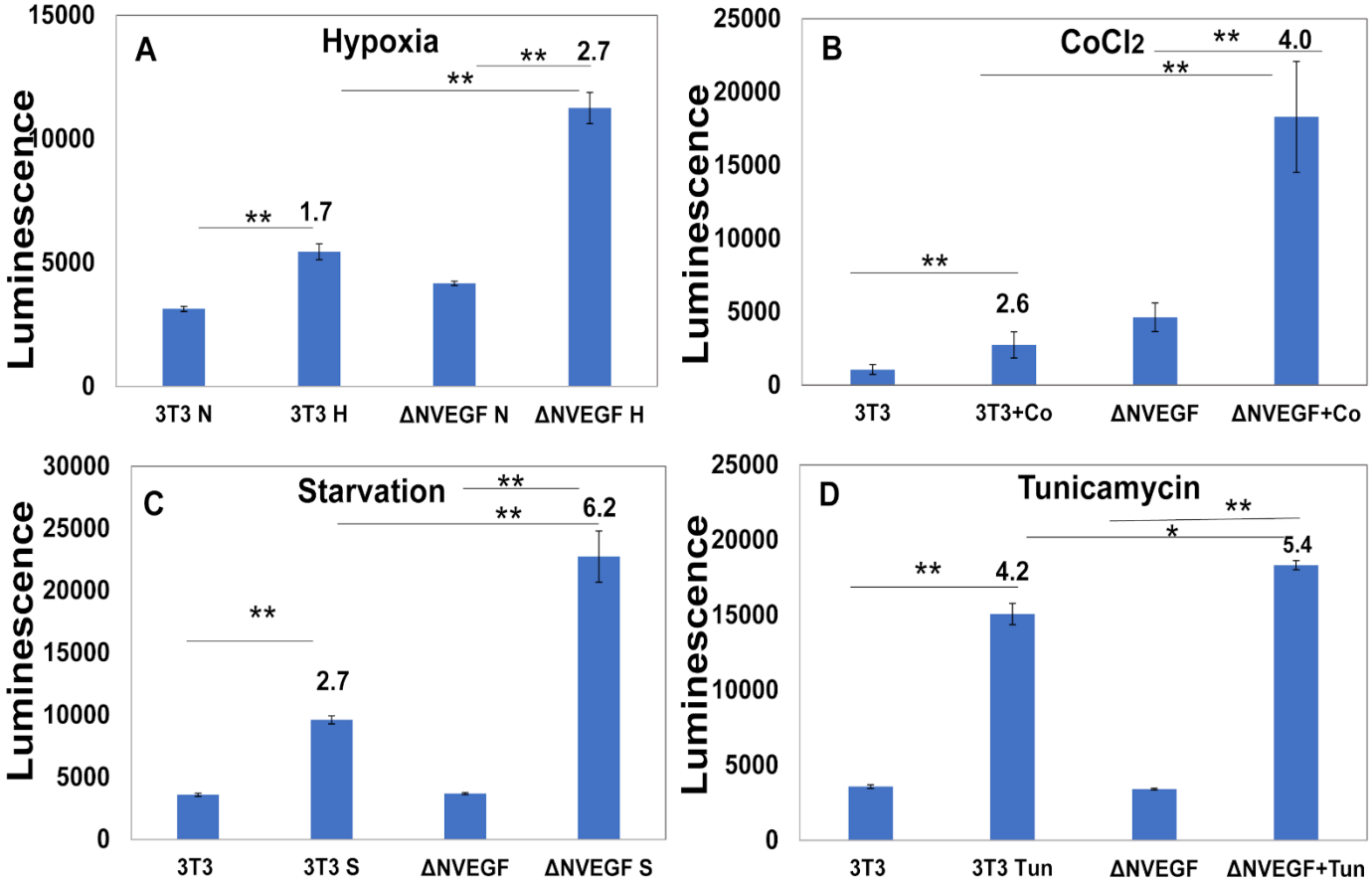

Fig. 9 Hypoxia, cell starvation, and exposure to cobalt chloride lead to increased apoptosis in ΔN-VEGF cells in comparison to NIH3T3 cells. To determine apoptosis in ΔN-VEGF cells in comparison to NIH3T3 cells following different stress signals, The ApoTox-Glo™ Triplex Assay measuring relative apoptosis was utilized. To induce stress signals, cells were treated with (A) hypoxia, (B) $CoCl_2$, (C) starvation and (D) Tunicamycin. Cells were either cultured under normoxia or hypoxia for 18 hrs. Subsequently, caspase reagents were added to the plate and the plate was incubated at RT for an additional 1.5 hrs and luminescence was then measured. The results represent three different experiments that were performed in triplicates. Statistical significance was determined by Student's t-test, * $p<0.05$, ** $p<0.01$).

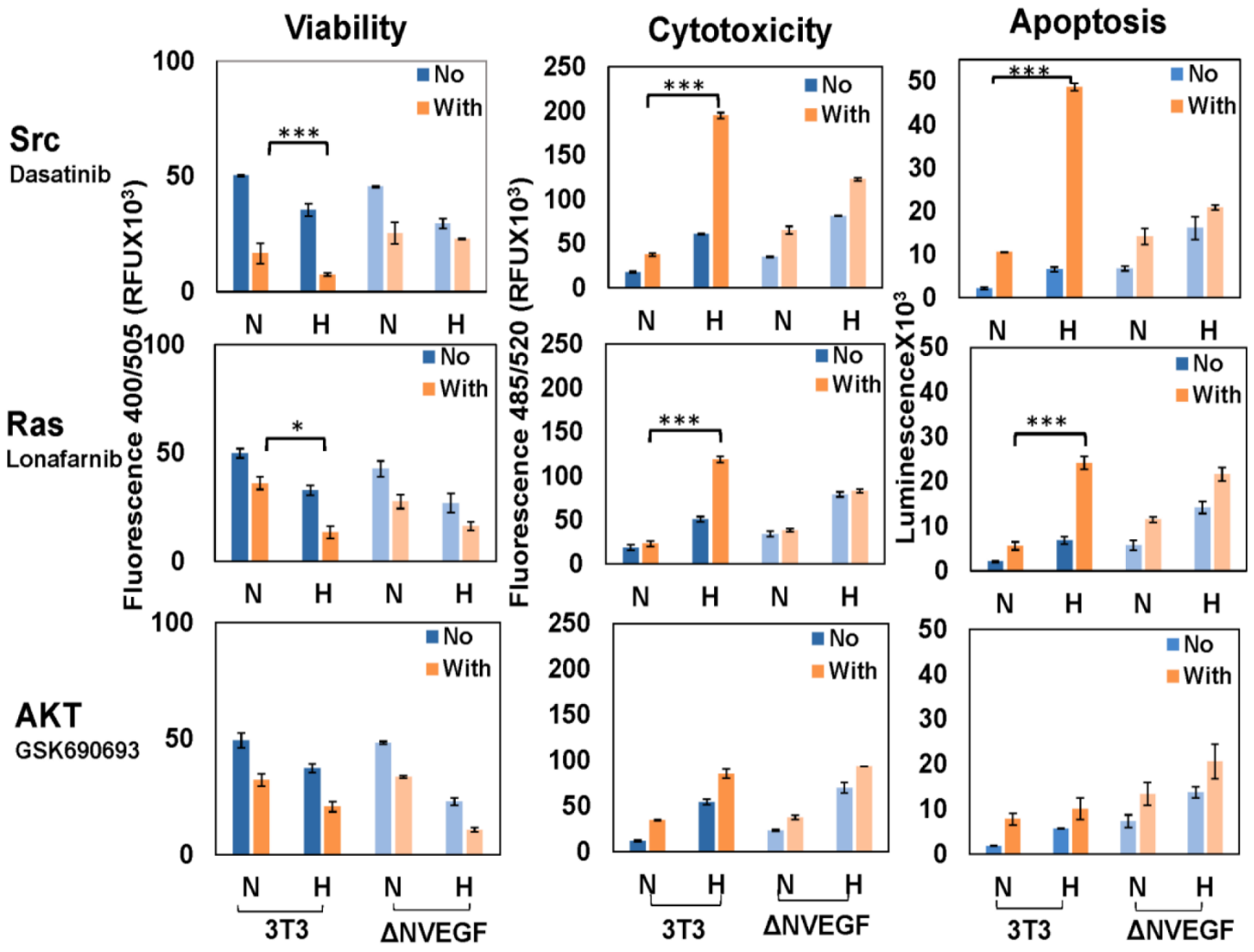

Fig. 10 The effect of Src, Ras and AKT inhibitors on the viability, cytotoxicity, and apoptosis of NIH3T3 cells. NIH3T3 and ΔN-VEGF cells were subjected to hypoxia in the presence or the absence of the Dasatinib (1μM), Lonafarnib (15μM) and GSK690693 (25μM), inhibitors of Src, Ras and AKT, respectively. Viability, cytotoxicity, and apoptosis were determined using the ApoTox-Glo™ Triplex Assay as detailed under Materials and methods. Three independent experiments were performed in triplicates. Statistical significance for this figure is detailed under Materials and methods. determined by Two-way ANOVA followed by Tukey's HSD test, * $p<0.05$, *** $p<0.001$.

Supporting information

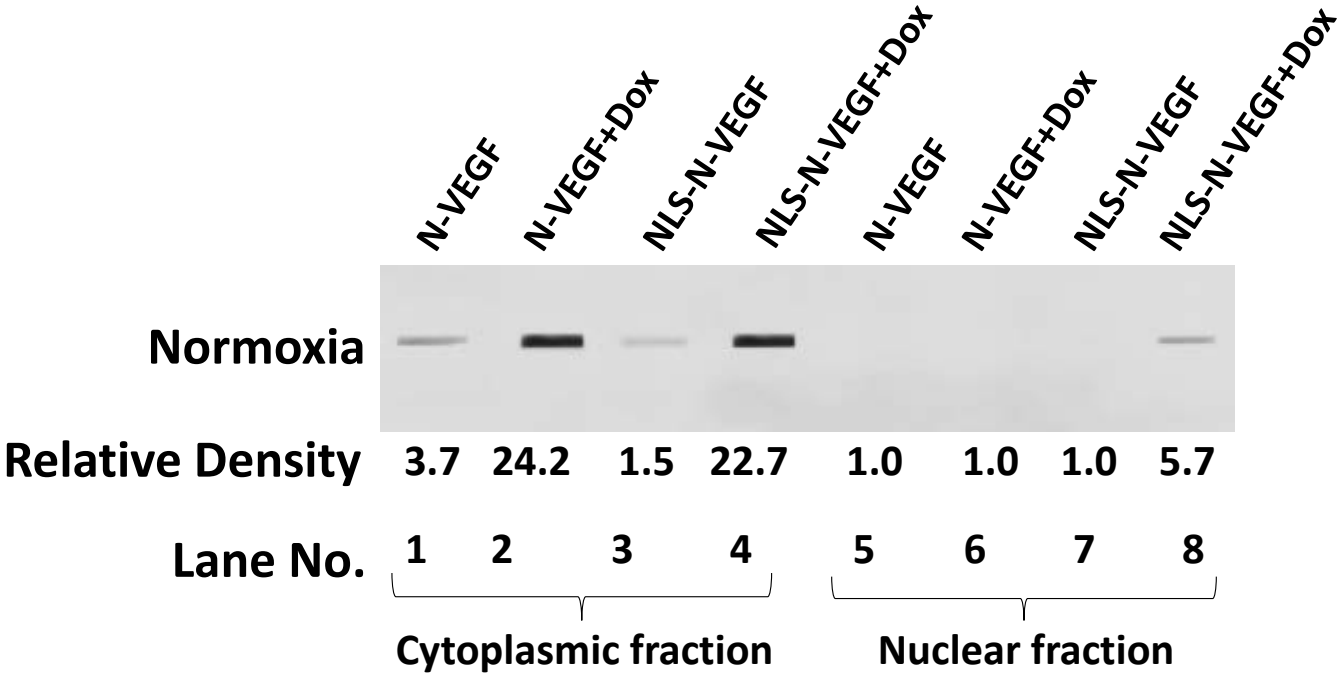

Fig. S1. Relative densities of N-VEGF and NLS-N-VEGF. This is a supplementary data for Fig.1 showing relative density in each lane generated by ImageJ web service program.

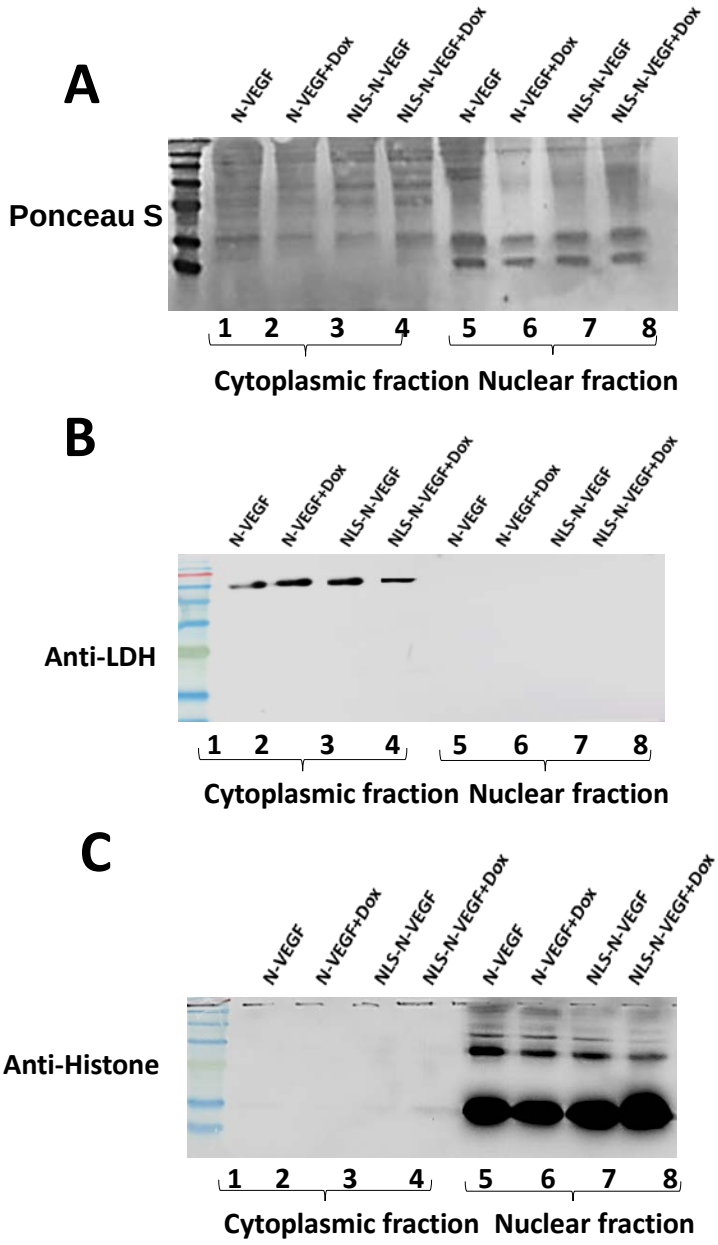

Fig. S2. Supplementary material for Fig. 1. Western blot was performed as described under Fig. 1. **(A)** Ponceau S staining of membrane prior to blocking and exposure to antibodies to demonstrate equal protein loading for all cytoplasmic and nuclear fractions. **(B)** The Western blot membrane was stripped from the first N-VEGF directed antibodies and Western blot with polyclonal antibodies directed against LDH, a cytoplasmic specific protein. Western blot analysis was performed as detailed under Fig. 1. **(C)** The Western blot membrane was stripped from the LDH directed antibodies and Western blot with polyclonal antibodies directed against histone H3, a nuclear specific protein. Western blot analysis was performed as detailed under Fig.1.

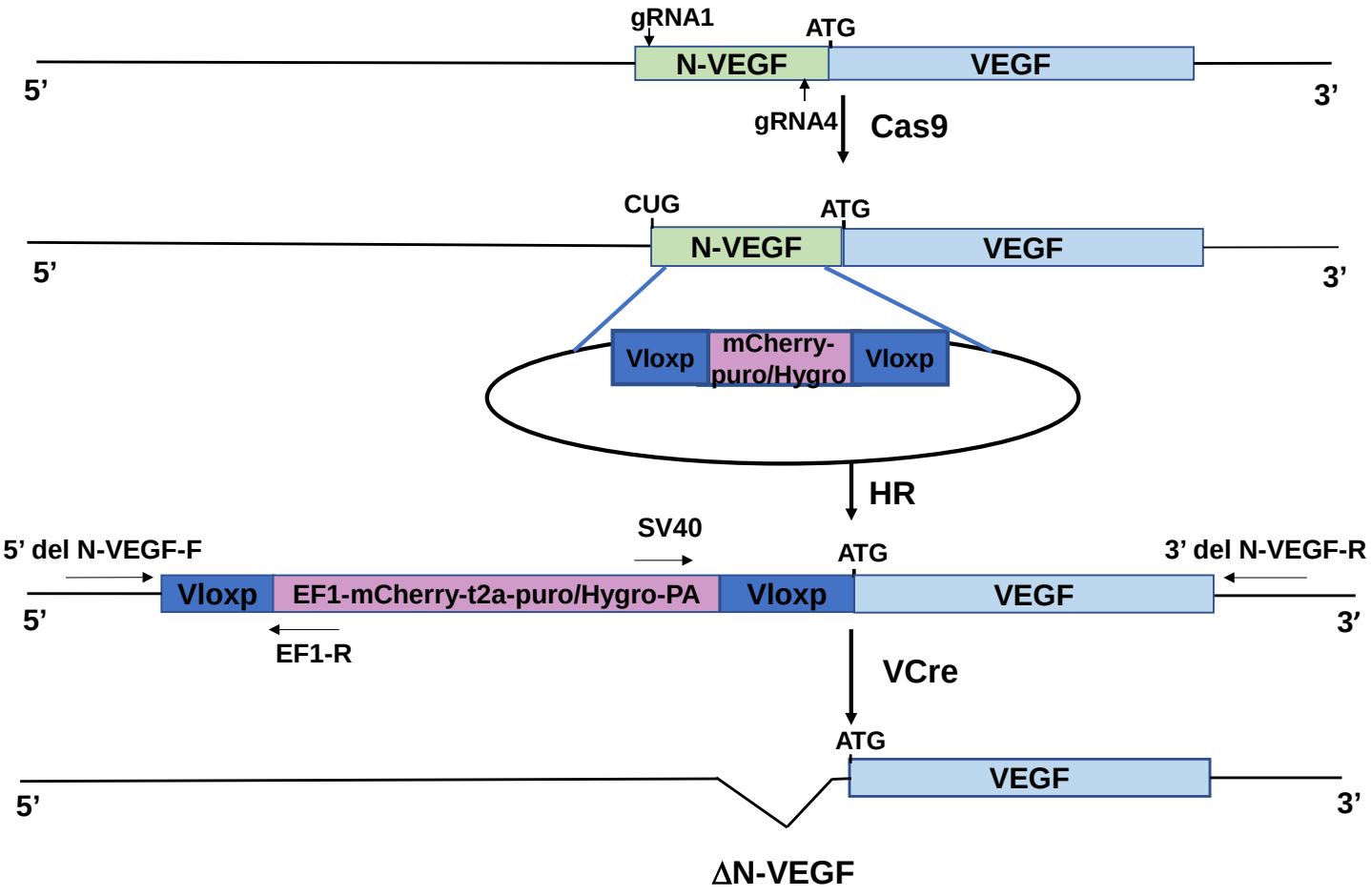

Fig. S3. Schematic illustrations. Schematic illustration of the two-steps protocol for CRISP-Cas9 mediated biallelic deletion of N-VEGF.

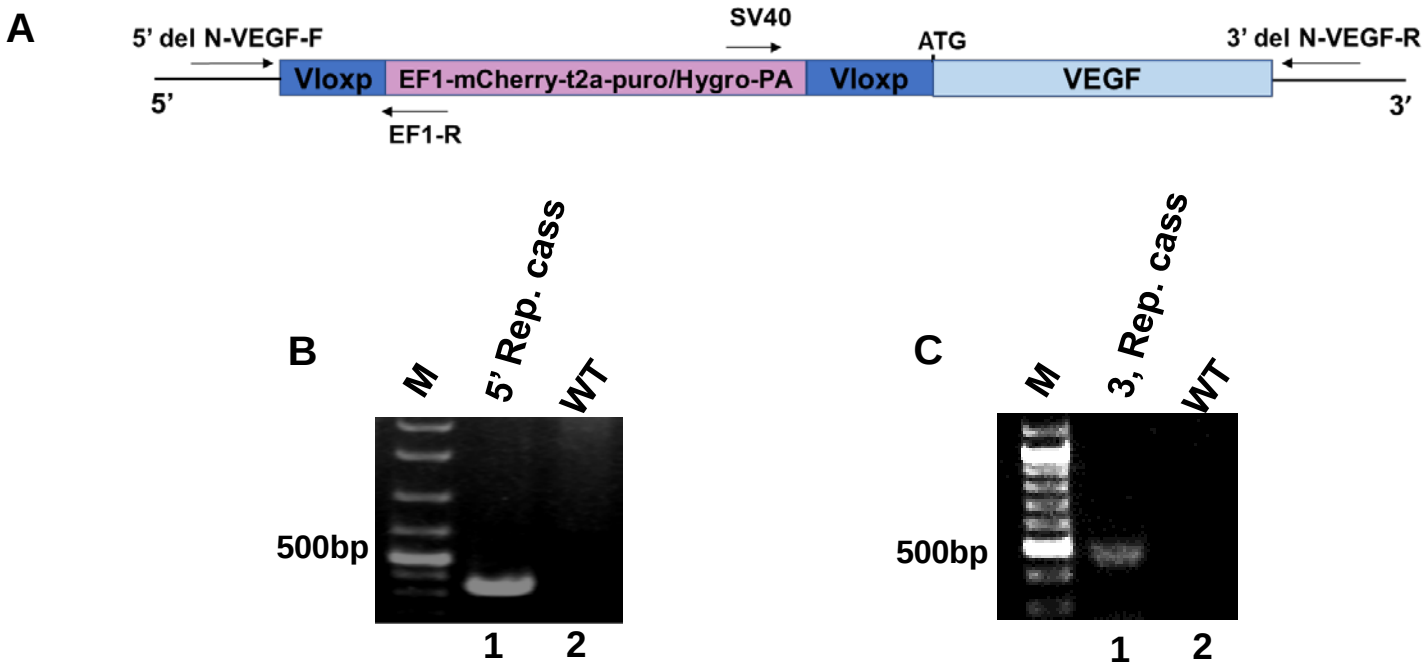

Fig. S4. PCR analysis of NIH3T3 with a replacement of the N-VEGF gene with a reporter cassette. (A) Schematic illustration of the reporter cassette harboring a reporter gene followed by Puromycin or Hygromycin resistance genes. Primer pairs for each junction were used for clones analysis. **(B)** Agarose gel showing the expected 435bp PCR product from 5' junction of isolated clone 1 (panel 1) obtained using the 5'-del NVEGF forward primer and reverse primer EF1-R from the insert. **(C)** Agarose gel showing levels of the expected 482bp PCR product from the 3' junction (panel 1), obtained using the SV40 forward primer and 3' del NVEGF reverse primer.

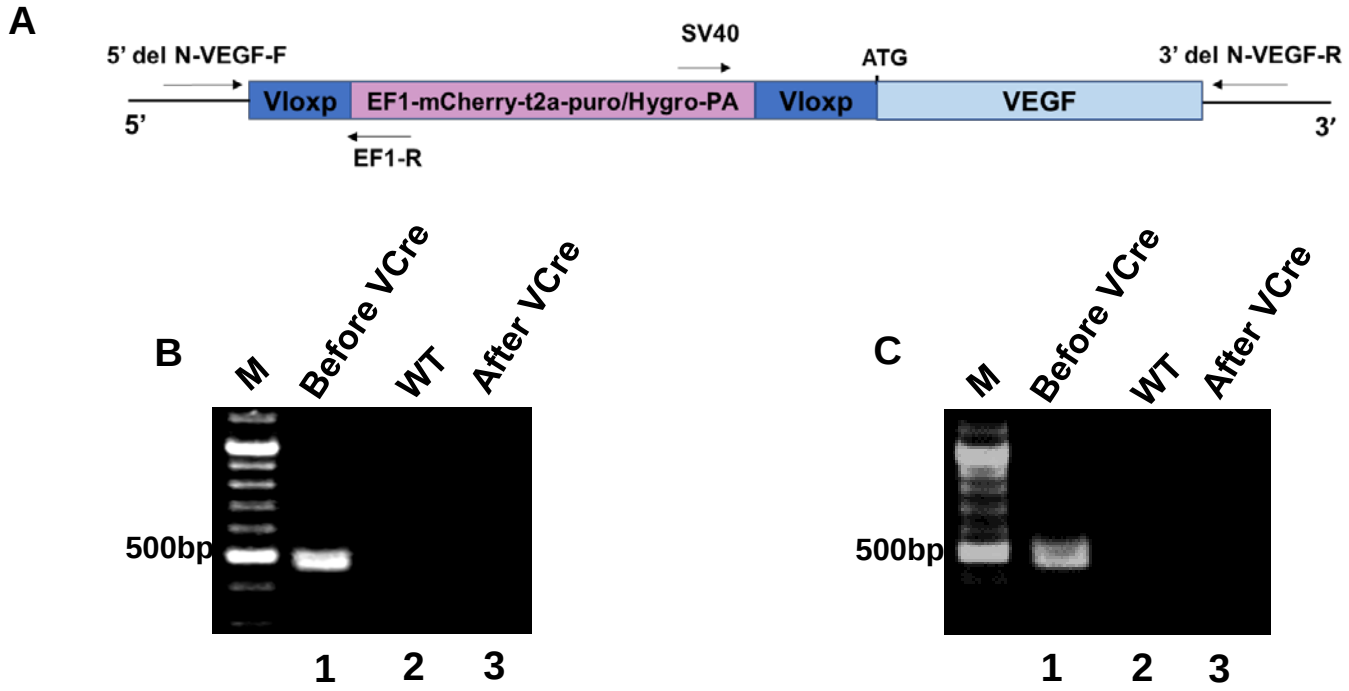

Fig. S5. PCR analysis to verify genomic N-VEGF deletion from NIH3T3. (A) Schematic illustration of the reporter cassette harboring a reporter gene followed by Puromycin or Hygromycin resistance genes. Primer pairs for each junction were used for clones analysis. **(B)** Agarose gel showing levels of the expected band of 435 bp PCR product from the 5' junction of clone 1 before (panel 1) and following VCre expression (panel 3). Removal of the reporter cassette was determined using 5'-del NVEGF forward primer and reverse primer EF1-R from the inset. **(C)** Agarose gel showing levels of the expected band of 482 bp PCR product from the 3' junction, obtained using the SV40 forward primer and 3'-del NVEGF reverse primer before (panel 1) versus after VCre expression (panel 3).

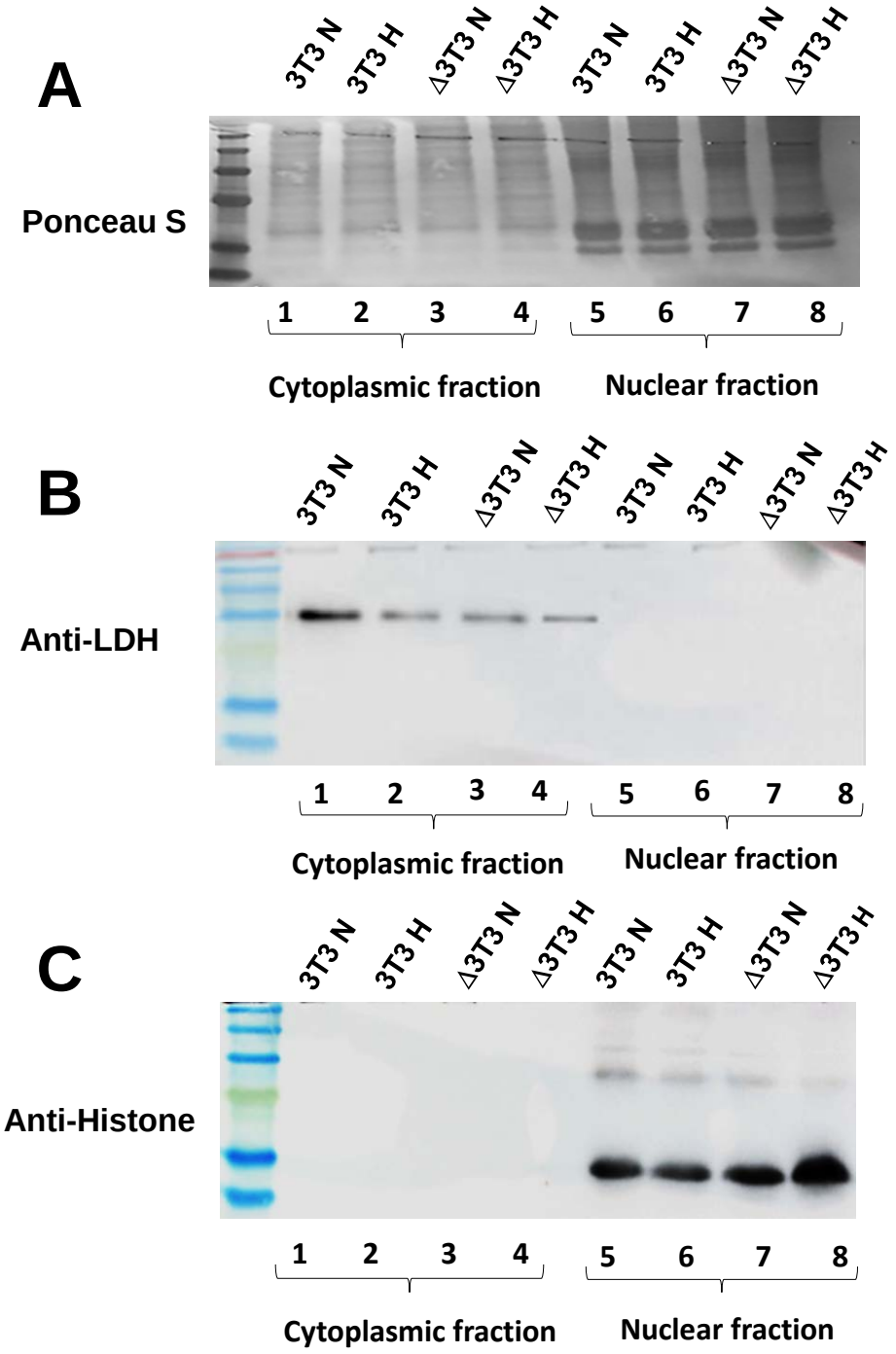

Fig. S6. Supplementary material for Fig. 4. (A) Ponceau S membrane staining and western blots with antibodies directed against anti LDH **(B)** and anti-histone H3 **(C)** were performed exactly as described under Fig. S2

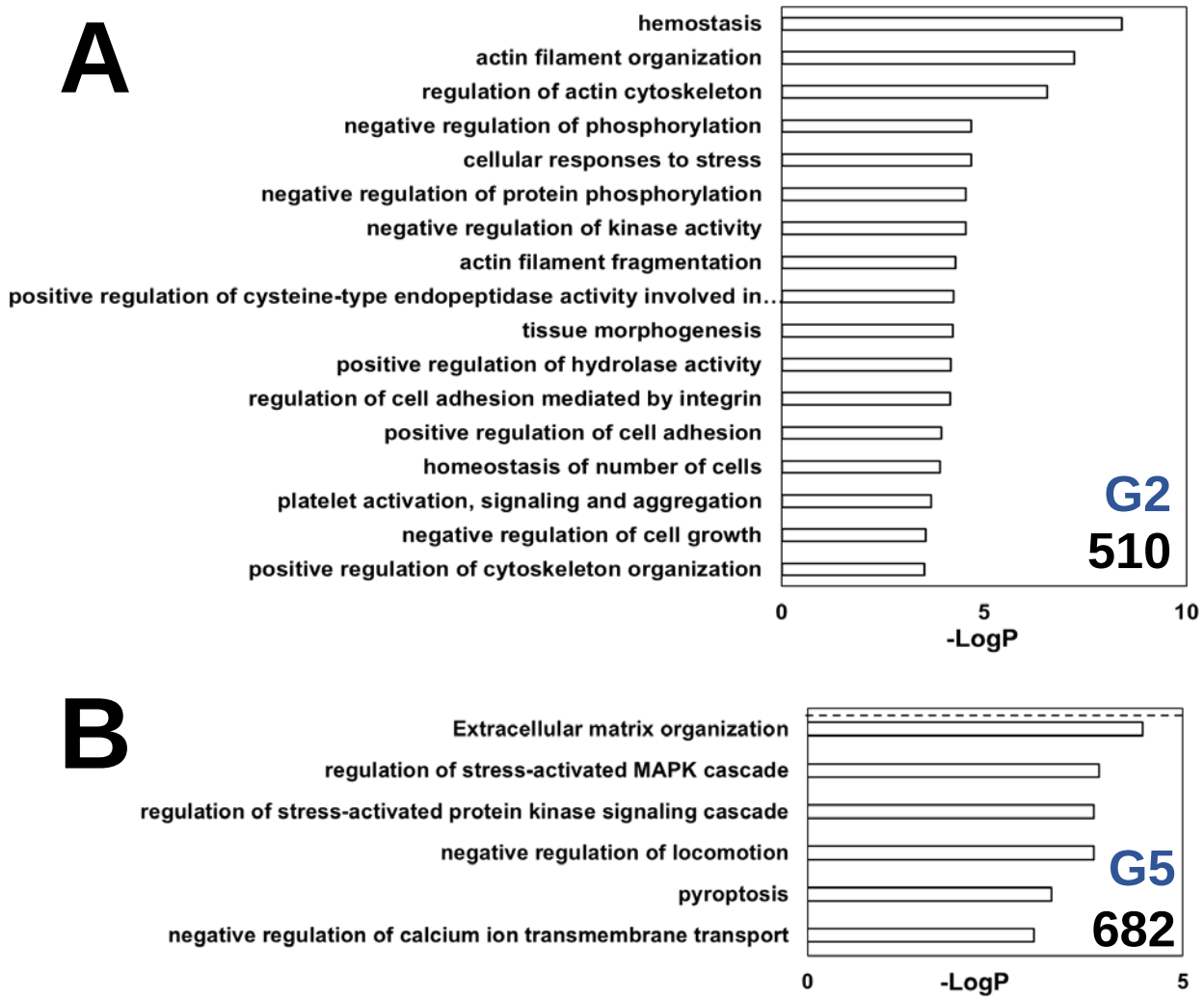

Fig. S7. Annotation of cluster G2 and G5. Annotation of genes that exhibited no change in expression pattern in ΔN-VEGF cells following hypoxia that were either upregulated **(A)** or downregulated **(B)** in NIH3T3 cells, cluster C2 and C5, respectively, are presented. Numbers on right lower corner of each bar graph represent the cluster number in blue and the genes number in the cluster in black.

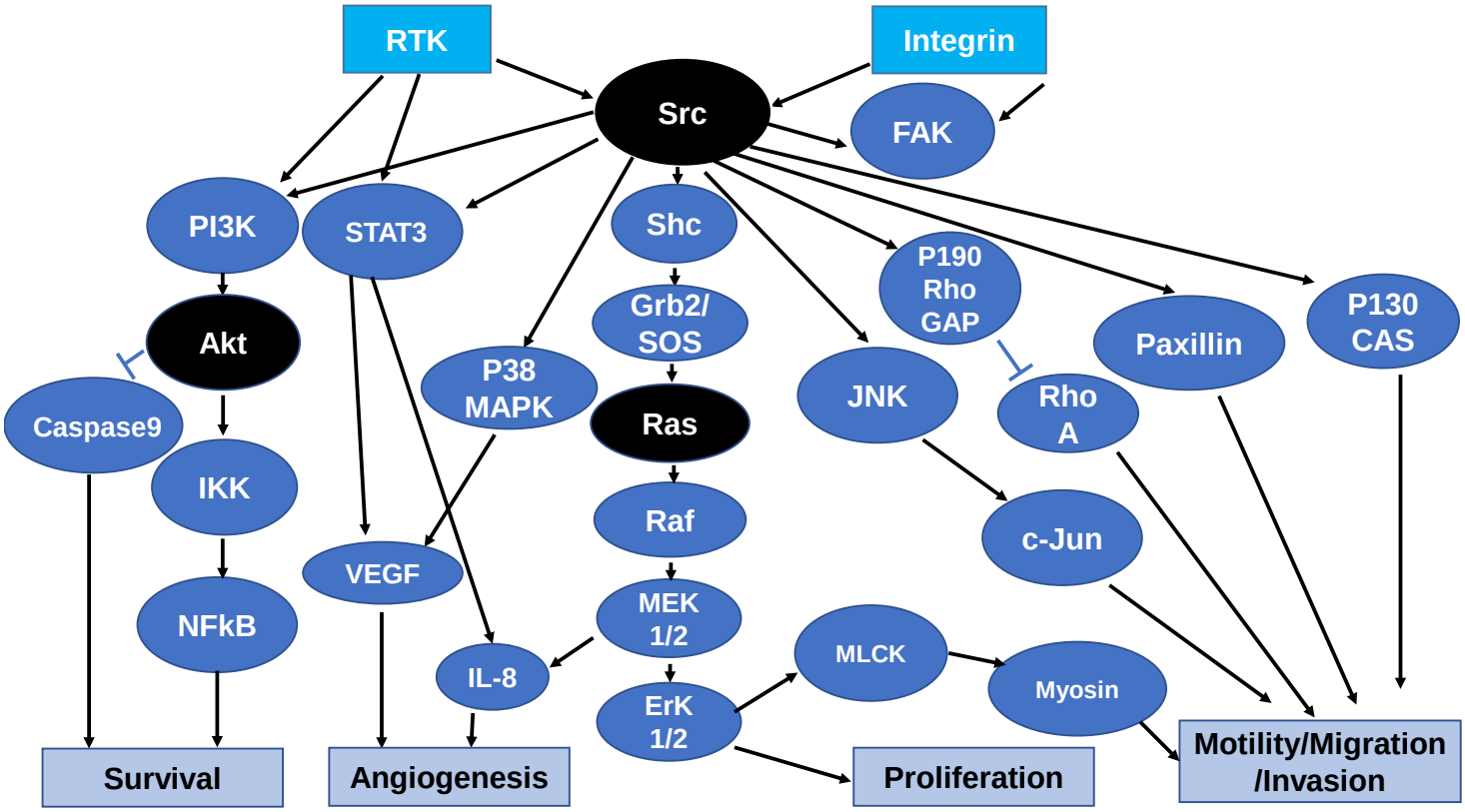

Adopted from: Summy and Gallick., Clin Cancer Res, 12: 1390-401, 2006

Fig. S8. Schematic illustration of the Src, Ras and AKT partial pathways

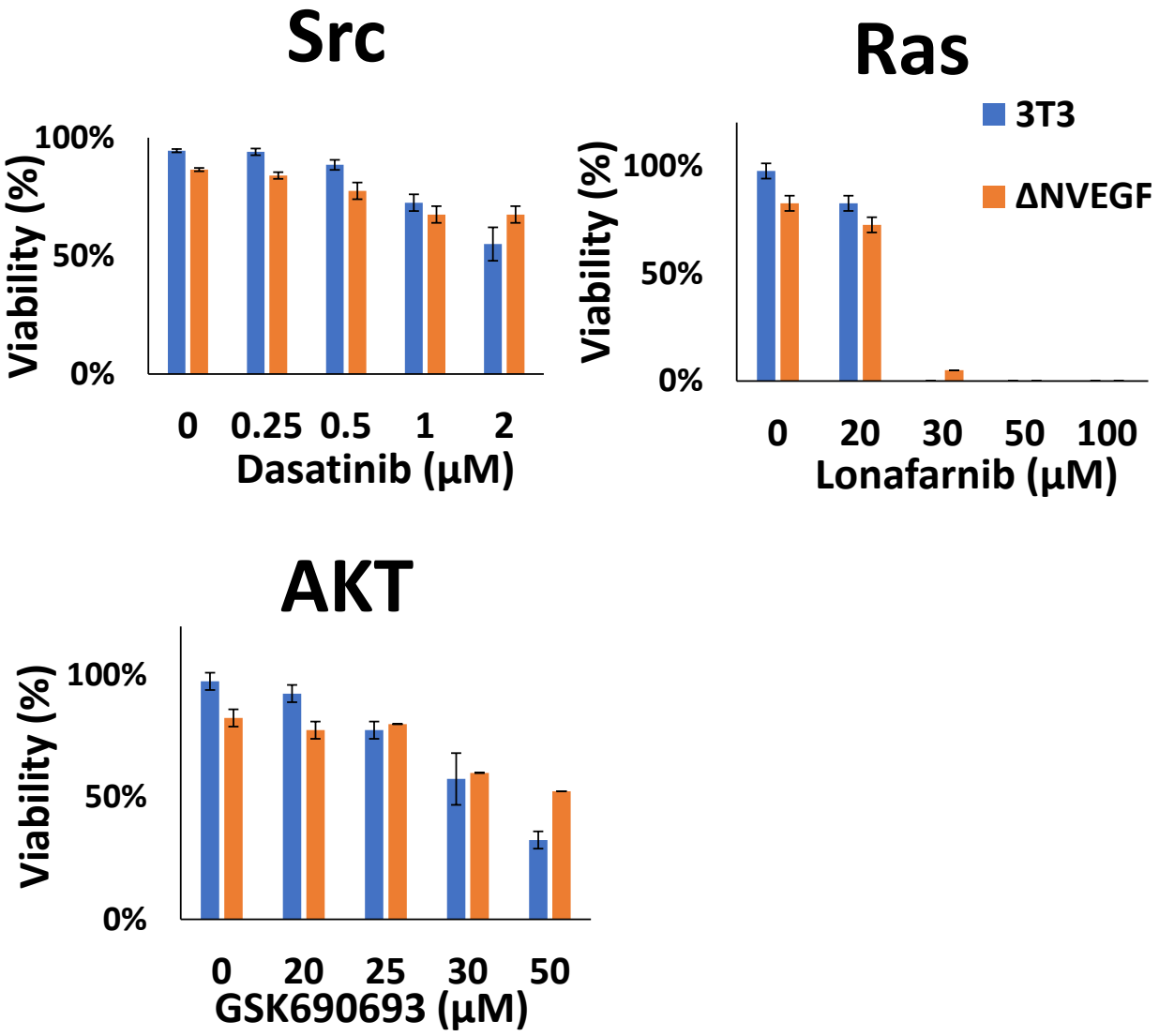

Fig. S9. Effect of Src, Ras and AKT inhibitors on cell viability. NIH3T3 and ΔN-VEGF cells were grown for 24 hrs under normoxia in the absence or the presence of various concentrations of Dasatinib (0.25, 0.5, 1,2 µM (62)), Lonafarnib (20, 30, 50,100 µM (63)) and GSK690693 (20, 25, 30, 50 µM (64)), inhibitors of Src, Ras and AKT, respectively. The effect on the viability of both cell types was evaluated by Trypan Blue staining assays. The inhibitor concentration that exhibited a reduction of about 20% in cell's viability yet, minimal difference in the viability level in both cell types, was chosen as detailed under Materials and Methods and in the text.

Table S1. Annotation of 155 genes the exhibited differential expression in NLS-N-VEGF cells treated with dox. Annotation of 123 upregulated genes (up tab) and 32 downregulated genes (down tab) in NLS-N-VEGF cells treated with dox.

Table S1.xlsx

Table S2. Annotation of genes that exhibited differential expression between Δ-N-VEGF and NIH3T3 cell following hypoxia. The genes are arranged in six groups (G1-G6). G1 and G6, similar expression pattern in both cell types of genes either induced or repressed following hypoxia, respectively. G3 and G4, inverse expression pattern in Δ-N-VEGF cells, either upregulated (G3) or downregulated (G4) following hypoxia in comparison to NIH3T3 under the same treatment. Last, genes that exhibited no change in expression pattern in ΔN-VEGF cells that were either upregulated or downregulated in NIH3T3 cells following hypoxia, groups G2 and G5, respectively. Statistically significant annotation groups, Log $q < 0.05$.

Table S2.xlsx

Table S3. List of primers used in this study.

Table S3.xlsx